Geochimica et Cosmochimica Acta Vol. 46, pp. 1627 to 1651

0016-7037/82/091627-25$03.00/0

Chemical composition of HAL, an isotopically-unusual Allende inclusion

ANDREW M. DAVIS[1], TSUYOSHI TANAKA[2] and LAWRENCE GROSSMAN[3]
Department of the Geophysical Sciences, The University of Chicago, 5734 South Ellis Avenue, Chicago, Illinois 60637

TYPHOON LEE[3]
Department of Terrestrial Magnetism, Carnegie Institution of Washington, 5241 Broad Branch Road, NW, Washington, D. C. 20015

and

G. J. WASSERBURG
Lunatic Asylum, Division of Geological and Planetary Sciences, California Institute of Technology, Pasadena, California 91109

(*Received July* 17, 1981; *accepted in revised form May* 6, 1982)

Abstract—Thirty-seven major, minor and trace elements were determined by INAA and RNAA in samples of hibonite, black rim and portions of friable rim from an unusual Allende inclusion, HAL. The peculiar isotopic, mineralogical and textural properties of HAL are accompanied by very unusual trace element abundances. The most striking feature of the chemistry is the virtual absence of Ce from an inclusion otherwise highly enriched in REE compared to C1 chondrites. HAL is also depleted in Sr, Ba, U, V, Ru, Os and Ir, relative to other refractory elements. Of the lithophile elements determined which are normally considered to be refractory in a gas of solar composition, Sr, Ba, Ce, U and V are the most volatile in oxidizing gases. The distribution of REE between hibonite and rims seems to have been established when hibonite and other refractory minerals were removed at slightly different temperatures from a hot, oxidizing gas in which they previously coexisted as separate grains. On the basis of HAL's chemical and isotopic composition, possible locations for the chemical and mass dependent isotopic fractionation are in ejecta from the low temperature helium-burning zone of a supernova and in the locally oxidizing environment generated by evaporation of interstellar grains of near-chondritic chemical composition.

INTRODUCTION

A HIBONITE-RICH inclusion first attracted the attention of one of us (T.L.) by its unusual, jewel-like appearance on a broken surface of the Allende C3 chondrite. Named HAL (for *H*ibonite *AL*lende), it has a texture that is distinctive among objects found in Allende. HAL consists of several large crystals of hibonite surrounded by a compact glassy black rim, which is, in turn, surrounded by a massive friable rim consisting of several mineralogically and texturally different layers.

HAL has an isotopic composition that places it among the FUN inclusions (Wasserburg *et al.*, 1977), a group characterized by a large number of unusual isotopic anomalies. Lee *et al.* (1979) reported substantial mass fractionation of calcium isotopes, favoring the heavy isotopes, upon which are superimposed small non-linear effects, presumably of nuclear origin. All samples of HAL have the same calcium isotopic composition. Despite $^{27}Al/^{24}Mg$ ratios in excess of 9000 (Allen *et al.*, 1980), no excess ^{26}Mg was found. Lee *et al.* proposed that HAL (1) condensed from a gas with isotopically normal magnesium and anomalous calcium, (2) was heated to such a high temperature that 50% of the calcium and virtually all of the magnesium were evaporated, (3) crystallized into hibonite and other refractory minerals and (4) reacted with a gas to form the black and friable rims. Lee *et al.* (1980) measured the isotopic composition of oxygen in HAL and concluded that hibonite suffered large mass fractionation of oxygen relative to the ^{16}O-rich reservoir from which most other Allende inclusions formed. Hibonite and related phases then back-reacted with the same, less ^{16}O-rich, reservoir with which normal Allende inclusions reacted. Hibonite is enriched in the heavy isotopes of oxygen, consistent with the conclusion reached by Lee *et al.* (1979) that the material from which hibonite formed suffered substantial evaporative mass loss.

Allen *et al.* (1980) performed a detailed study of the mineralogy and petrology of HAL. They concluded that hibonite reacted partially with a melt which eventually quenched to form the black rim and that individual layers of the friable rim formed by accretion of condensate grains around HAL's nucleus rather than by wholesale reaction of a precursor of HAL with a nebular gas.

We report here the results of a detailed chemical study of HAL, which shows that the unusual history of this inclusion indicated by its textures, minerals

[1] Also: James Franck Institute, University of Chicago, 5640 South Ellis Avenue, Chicago, Illinois 60637 (present address).
[2] Present address: Geological Survey of Japan, Higashi 1-1-3, Yatabe, Ibaraki, 305 Japan.
[3] Also Enrico Fermi Institute, University of Chicago.

Table 1. Elemental abundances[1] in separated portions of HAL.

Sample	Description	Wt µg	Wt µg	Na_2O %	MgO %	Al_2O_3 %	SiO_2[2] %	CaO %	CaO %	Sc ppm
1	Hibonite, frosty core + clear margin	87.67 ±.08	35.20	0.0450 ±.0047	<2.9	90.32 ±.49	<1.6	9.17 ±.61	9.24 ±.71	561.4 ±.1
2	Hibonite, clear margin	21.32 ±.11	21.32	0.040 ±.016	<5.9	90.50 ±.75	<2.5	6.9 ±1.0	7.50 ±.68	451.9 ±.3
3	Black rim	9.79 ±.07	9.79	2.371 ±.076	11.7 ±4.1	58.14 ±.85	10.3 ±4.2	1.97 ±.85	2.06 ±.60	348.8 ±.1
4	Friable rim layers II, III and IV	24.31 ±.10	24.31	6.83 ±.12	<4.0	23.93 ±.36	28.1 ±2.6	19.3 ±1.6	19.4 ±2.1	704.5 ±.2
5	Friable rim layer V, with IV	3.61 ±.12	1.68	3.25 ±.16	<11	11.45 ±.98	44.7 ±5.8	22.1 ±4.6	22.1 ±4.6	2.702 ±.027
6	Friable rim layer V, with IV	18.39 ±.14	11.34	4.139 ±.087	13.0 ±2.1	12.54 ±.32	22.8 ±2.8	20.9 ±1.8	20.9 ±1.2	3.846 ±.014
7	Friable rim, bulk: layers I-V	103.65 ±.15	103.65	6.109 ±.095	9.76 ±.95	19.15 ±.17	32.6 ±1.2	13.30 ±.65	10.3 ±1.1	547.0 ±.3
Irradiation[3], Standard[4]		1	2 & 3	1,S	1,C	1,S		1,C	2,B	2,S
Isotope				^{24}Na	^{27}Mg	^{28}Al	By Diff.	^{49}Ca	^{47}Ca	^{46}Sc
Energy (keV)[5]				1368.5	1014.4	1778.9		3084.4	1297.1	889.3
Half-life[6]				15.020h	9.462m	2.259m		8.716m	4.536d	83.83d
C1 chondrites				0.6647	15.74	1.566		1.266	1.266	6.211

Sample	TiO_2 %	V ppm	Cr ppm	Mn ppm	Fe %	Co ppm	Ni ppm	Zn ppm	Br ppm	Sr ppm
1	0.45 ±.11	<28	41.1 ±2.5	12.9 ±1.2	0.1904 ±.0087	1.733 ±.028	<54	<19	<0.48	<210
2	0.83 ±.23	<57	<3.6	20.9 ±4.1	0.416 ±.010	2.967 ±.036	<47	81 ±16	<0.93	<285
3	2.82 ±.38	<73	41.2 ±1.1	1156 ±33	8.763 ±.020	24.45 ±.10	291 ±16	0.65% ±.13	<1.7	<53
4	10.78 ±.26	<32	38.6 ±3.7	897 ±24	8.178 ±.027	58.62 ±.13	555 ±40	149 ±30	9.6 ±1.2	27 ±13
5	1.72 ±.64	<92	1623 ±8	2368 ±73	12.26 ±.05	181.0 ±.7	3367 ±42	184 ±57	<2.1	
6	<0.41	<33	1561 ±5	2002 ±52	18.56 ±.05	449.2 ±.7	9340 ±83	245 ±49	5.55 ±.75	
7	4.274 ±.095	23.9 ±7.0	799.2 ±2.5	1095 ±28	10.83 ±.02	164.7 ±.2	3331 ±30	353 ±71	8.25 ±.87	16.9 ±1.4
Irr.[3], Std.[4]	1,C	1,S	2,S	1,S	2,S	2,S	2,S	2,B	2,S	2,S
Isotope	^{51}Ti	^{52}V	^{51}Cr	^{56}Mn	^{59}Fe	^{60}Co	^{58}Co	^{65}Zn	^{82}Br	^{85}Sr
Energy (keV)[5]	319.8	1433.9	320.0	846.6	1099.2	1332.5	810.8	1115.5	554.3	514.0
Half-life[6]	5.76m	3.75m	27.704d	2.5785h	45.1d	5.271y	70.76d	244.1d	35.30h	65.19d
C1 chondrites	0.0741	55.5	2594	1912	18.07	502.5	10270	301	3.22	7.38

Sample	Zr %	Ru ppm	Cs ppm	Ba ppm	La ppm	La ppm	Ce ppm	Ce ppm	Nd ppm	Nd ppm	Sm ppm
1	<0.014	<2.3	<0.12	5.2 ±1.7	13.42 ±.09	11.59 ±.06	<1.4	<0.11	<26	14.95 ±.69	3.369 ±.009
2	<0.0065	<1.9	<0.12	<8.9	12.83 ±.18	12.74 ±.06	<2.9	<0.14	37 ±15	16.45 ±.95	3.420 ±.030
3	0.0232 ±.0051	<1.3	0.216 ±.078	21.9 ±8.5	4.419 ±.064	3.544 ±.043	<0.89	0.300 ±.093	<9.7	9.39 ±.98	3.645 ±.016
4	0.124 ±.010	3.0 ±1.5	<0.10	9.1 ±4.4	16.65 ±.26	16.52 ±.09	<2.1	0.39 ±.12	<68	47.9 ±2.0	17.67 ±.04
5	0.0234 ±.0092	<2.6	<0.36		<0.37		<4.0		<18		<0.080
6	<0.0088	<1.0	<0.17		<0.39		<1.0		<7.1		0.076 ±.018
7	0.0336 ±.0060	<1.6	0.162 ±.023	21.52 ±.88	6.24 ±.15	6.538 ±.038	<1.1	0.528 ±.062	<40	19.8 ±1.4	6.721 ±.021
Irr.[3], Std.[4]	2,S	2,C	2,S	3,S	2,C	3,C	2,C	3,C	2,C	3,C	2,C
Isotope	^{95}Zr	^{103}Ru	^{134}Cs	^{131}Ba	^{140}La	^{140}La	^{141}Ce	^{141}Ce	^{147}Nd	^{147}Nd	^{153}Sm
Energy (keV)[5]	756.7	497.0	795.8	123.7 & 496.3	1596.4	1596.4	145.4	145.4	531.4	531.4	103.2
Half-life[6]	63.98d	39.35d	20.62y	11.8d	40.272h	40.272h	32.50d	32.50d	10.98d	10.98d	46.7h
C1 chondrites	3.44ppm	0.721	0.192	2.3	0.2452	0.2452	0.6368	0.6368	0.4688	0.4688	0.1526

Table 1 (cont'd). Elemental abundances[1] in separated portions of HAL.

Sample	Sm ppm	Eu ppm	Eu ppm	Gd ppm	Tb ppm	Tb ppm	Dy ppm	Dy ppm	Tm ppm	Tm ppm
1	2.935 ±.007	0.999 ±.018	1.098 ±.034	<5.4	0.257 ±.048	0.269 ±.010	1.086 ±.083	1.342 ±.024	<0.15	0.042 ±.014
2	3.590 ±.006	0.915 ±.021	0.962 ±.025	<7.8	0.284 ±.048	0.327 ±.012	1.34 ±.28	1.460 ±.036	<0.14	0.040 ±.015
3	2.619 ±.009	0.766 ±.042	1.044 ±.048	<6.3	0.966 ±.051	0.637 ±.012	7.0 ±1.0	5.113 ±.051	0.752 ±.063	0.506 ±.016
4	18.20 ±.02	2.567 ±.025	2.790 ±.036	24.1 ±6.2	4.157 ±.099	4.795 ±.016	32.1 ±1.3	37.84 ±.13	3.73 ±.12	3.419 ±.017
5		<0.040			<0.48		<5.4		<0.44	
6		<0.077			<0.21		<2.1		<0.10	
7	7.099 ±.007	1.133 ±.009	1.626 ±.020	12.6 ±3.3	1.635 ±.058	2.072 ±.006	15.62 ±.56	16.04 ±.05	1.574 ±.062	1.525 ±.006
Irr.[3], Std.[4]	3,C	2,C	3,C	3,C	2,C	3,C	1,S	3,C	2,C	3,C
Isotope	^{153}Sm	^{152}Eu	^{152}Eu	^{159}Gd	^{160}Tb	^{160}Tb	^{165}Dy	^{166}Dy	^{170}Tm	^{170}Tm
Energy (keV)[5]	103.2	1408.0	1408.0	363.6	1177.9	298.6	94.7	82.5	84.3	84.3
Half-life[6]	46.7h	13.2y	13.2y	18.56h	72.3d	72.3d	2.334h	81.6h	128.6d	128.6d
C1 chondrites	0.1526	0.05750	0.05750	0.2002	0.03798	0.03798	0.2504	0.2504	0.02502	0.02502

Sample	Yb ppm	Yb ppm	Lu ppm	Lu ppm	Hf ppm	Ta ppm	Os ppm	Ir ppm	Au ppm	Th ppm	U ppm
1	0.32 ±.12	0.2646 ±.0089	<0.051	0.0493 ±.0028	1.996 ±.087	0.216 ±.049	<0.85	0.6488 ±.0083	<0.012	<0.28	<0.19
2	0.41 ±.15	0.2408 ±.0097	<0.099	0.0486 ±.0047	1.746 ±.080	0.289 ±.051	1.75 ±.49	2.537 ±.008	<0.020	<0.23	<0.49
3	4.293 ±.093	2.909 ±.021	0.684 ±.053	0.5143 ±.0049	5.386 ±.065	0.645 ±.052	<0.36	0.0990 ±.0048	<0.017	1.041 ±.074	<0.99
4	21.73 ±.42	21.39 ±.05	4.240 ±.090	4.019 ±.014	23.66 ±.15	3.328 ±.072	<1.8	1.368 ±.011	<0.045	4.28 ±.21	<0.48
5	<0.60		<0.10		<0.52	<0.53	<0.86	0.0518 ±.0094	0.073 ±.025	<0.53	
6	<0.27		<0.039		0.318 ±.056	<0.18	0.47 ±.16	0.2125 ±.0034	0.035 ±.015	<0.21	
7	9.02 ±.22	9.378 ±.024	1.986 ±.047	1.903 ±.007	9.699 ±.077	1.321 ±.035	1.04 ±.39	0.6030 ±.0056	0.051 ±.013	1.39 ±.10	0.123 ±.045
Irr.[3], Std.[4]	2,C	3,C	2,C	3,C	2,S	2,S	2,C	2,C	2,C	2,S	3,S
Isotope	^{175}Yb	^{175}Yb	^{177}Lu	^{177}Lu	^{181}Hf	^{182}Ta	^{191}Os	^{192}Ir	^{198}Au	^{233}Pa	^{140}Ba
Energy (keV)[5]	396.3	396.3	208.4	208.4	133.0	1221.4	129.4	468.1	411.8	311.9	487.0 (^{140}La)
Half-life[6]	4.19d	4.19d	6.71d	6.71d	42.4d	115.0d	15.4d	74.02d	2.696d	27.0d	12.746d
C1 chondrites	0.1658	0.1658	0.02498	0.02498	0.117	0.014	0.515	0.485	0.142	0.0286	0.0082

[1]Errors given are 1σ uncertainties based on counting statistics alone. Additional uncertainties in INAA and RNAA are estimated to be <3% and <6%, respectively (see text). [2]This value includes significant amounts of P_2O_5 in samples 3, 4 and 7 and S in samples 5, 6 and 7. [3]1 indicates data determined *via* the short INAA irradiation; 2, the long INAA irradiation; and 3, the RNAA irradiation. [4]B indicates use of USGS standard rock BCR-1; C, use of a chemical standard; and S, use of Standard Pottery SP. [5]Bowman and McMurdo (1974). [6]Half-lives are taken from the most recent entry in *Nuclear Data Sheets*.

and isotopic composition is reflected in a number of exceptional chemical peculiarities. We will explore models for the formation of HAL that are consistent with all available data.

EXPERIMENTAL

HAL is a subspherical inclusion with a maximum diameter of 5 mm. Detailed mineralogical and textural descriptions of all zones can be found in Allen *et al.* (1980) and will only be summarized here. HAL consists of three texturally distinct portions: (1) several coarse hibonite crystals surrounded by (2) a narrow vitreous black rim which is surrounded by (3) a thicker multi-layered fine-grained friable rim. Each hibonite crystal has a frosty core enclosed by a clear outer zone. The frosty appearance of the core is caused by extremely fine needles of a titanium-rich mineral, possibly rutile. The major phase in the black rim is a devitrified glass, rich in aluminum and iron. This phase will hereafter be referred to as aluminum iron oxide. Minor nepheline, sodalite and anorthite are also present in the black rim. The friable rim consists of five texturally and mineralogically distinct layers which have been labelled I through V by Allen *et al.* Friable rim layer I is approximately 50 μm thick and contains nepheline, sodalite, aluminum iron oxide, anorthite and an unknown titanium iron oxide phase. Layer II is approximately 100 μm thick and contains nepheline, aluminum iron oxide, perovskite, grossular, andradite, sodalite, calcium magnesium iron pyroxene and titanium iron oxide. Layer III is approximately 30 μm thick and contains calcium phosphate (possibly hy-

Table 2. Comparison of electron microprobe (Allen *et al.*, 1980) with INAA (this work) analyses of interior hibonite. All analyses are given in wt%. Errors in INAA are as in Table 1.

	Electron microprobe	INAA	
		Frosty core + clear margin	Clear margin
MgO	<0.01	<2.9	<5.9
Al_2O_3	89.95(88.07-91.00)	90.32±.49	90.50±.75
SiO_2	<0.02(<0.02-0.04)	<1.6	<2.5
CaO	8.71(8.32-9.02)	9.24±.71	7.50±.68
Sc_2O_3	0.05(<0.03-0.09)	0.08611±.00002	0.06931±.00002
TiO_2	0.71(0.60-1.06)	0.45±.11	0.83±.23
V_2O_3	<0.02	<0.0041	<0.0084
Cr_2O_3	<0.02	0.00601±.00037	<0.00053
FeO	0.32(0.20-0.43)	0.245±.011	0.535±.013
ZrO_2	<0.02(<0.02-0.03)	<0.019	<0.0088

droxyapatite), perovskite, nepheline and grossular-andradite intergrowths. Layer IV is approximately 50 μm thick and contains grossular-andradite intergrowths, perovskite, nepheline, hibonite, aluminum iron oxide, titanium iron oxide, pyroxene and an unknown titanium scandium zirconium oxide phase. Rim layer V is approximately 1.6 mm thick and contains nepheline, olivine, grossular-andradite intergrowths, pyroxene, aluminum iron oxide, sodalite, pentlandite, nickel-iron metal, titanium iron oxide and perovskite.

The inclusion was removed from the meteorite by G. J. W. at Caltech using stainless steel and tungsten tools. Portions of all zones sampled were then sent to Chicago for further selection. A total of seven samples for chemical analysis were handpicked under a microscope with stainless steel dental tools and a tungsten needle. All sample handling was done in clean rooms. A brief description of each sample follows.

Sample 1 was a fragment of a single hibonite crystal with roughly equal portions of clear margin and frosty core and contained no visible black rim. Sample 2 was a portion of the clear margin of the same hibonite crystal from which sample 1 was taken and contained no visible frosty hibonite or black rim. Sample 3 consisted of four fragments of black rim and contained no visible interior hibonite or exterior friable rim. Sample 4 was a single fragment of friable rim layers II, III and IV. Samples 5 and 6 were single fragments of rim layer V which may have contained small amounts of rim layer IV. Sample 6 contained some white patches, while sample 5 was free of them. Sample 7 was a single chip of bulk friable rim containing rim layers I through V. The relative proportions of rim layers in sample 7 were probably not the same as seen by Allen *et al.* (1980) in thin section, due to the irregular shape of the chip.

Each sample was weighed five times with a Perkin-Elmer AD-2Z electronic microbalance. The samples weighed from 3.61 to 103.65 μg each. The relative standard deviation was 3.3% for the smallest sample and less than 1% for the remaining samples. All chemical analyses of HAL were done by neutron activation. Details of the techniques used are given in the Appendix.

RESULTS

The results are shown in Table 1, along with standards, isotopes, γ-ray energies and half-lives used and C1 chondrite normalization values. Blank corrections for polyethylene pouches were made when necessary. No blank corrections were necessary for the long INAA or RNAA irradiations because the samples were transferred from their irradiation vials following these irradiations. The errors given in Table 1 are 1σ uncertainties based on counting statistics alone, except for zinc and lutetium. Calculation of errors for the latter elements are discussed in the Appendix. Additional uncertainties due to uncorrected neutron flux variations and counting geometry variations are estimated to be less than 3%. Uncertainty in rare earth element (REE) chemical yields contributes an additional uncertainty of less than 5% to the RNAA-determined REE abundances.

One important assumption in chemical analysis by neutron activation is that samples and standards have the same isotopic composition. The validity of this assumption can be questioned for HAL, since two of the three elements for which isotopic analyses have been performed show anomalies. However, the oxygen and calcium isotopic anomalies are only of the order of a few percent, while the elemental fractionations discussed in this paper are much larger.

The high purity of the hibonite samples allowed direct comparison of INAA results with the electron microprobe analyses of Allen *et al.* (1980) (Table 2). This is the first opportunity we have had to test our INAA method for determination of major elements in tiny samples. It can be seen that the agreement between the two methods is excellent.

In Table 3, our INAA and RNAA analyses of REE in the two standard rock samples are compared with the INAA data of Perlman and Asaro (1971) for SP and the mass spectrometric isotope dilution analyses of Nakamura (1974) for BCR-1. The good agreement between our INAA data and the literature values is caused in part by our use of literature values to correct our raw data for sample loss (see Appendix). The fact that there is no systematic difference between our SP data and the literature values across the REE series suggests that no REE fractionation accompanied sample loss. For BCR-1, however, heavy REE are enriched in our sample relative to light REE, compared to literature values. This may be due to fractionation of REE-bearing minerals when portions of BCR-1 were lost during transfers. The good agreement between our RNAA data and literature values is more significant, as sample loss was corrected for by a method which is independent of that used for the INAA data and independent of REE as well. Again, little fractionation of REE during sample loss is indicated by the SP data, while slight heavy REE enhancement is evident in the data for BCR-1. We conclude that there are no major problems with our method for determination of REE chemical yields and that the very unusual REE patterns of HAL are not artifacts of our analytical techniques.

Comparison of INAA with RNAA analyses of REE (Table 1) shows good agreement between the two techniques for most REE and most samples. The RNAA results for samples 1 and 3 are ~15% and ~25%, respectively, lower than the INAA results. These differences may be due to undetected sample loss during transfers and uncorrected neutron flux variations in the INAA, RNAA and chemical yield irradiations. Sample 1 was a single piece, so sample loss seems unlikely for it. It is conceivable that one of the four fragments that comprised sample 3 was lost during transfer. Since there was less opportunity for the above two sources of inaccuracy to affect the INAA data, the RNAA data were normalized to the INAA data by multiplying the RNAA-determined REE concentrations in each sample by the INAA/RNAA concentration ratio of lanthanum for that sample. The results so obtained (Table 4) allow comparison of INAA data for other elements with the best possible REE data. After normalization, substantial disagreements between RNAA and INAA analyses remain for europium in samples 3 and 7. The flux corrections for europium in this work are strongly dependent on neutron capture cross-sections, total neutron fluence and the fluence received by each sample (see Appendix). Errors in some or all of these values are believed to be the cause of the discrepant europium values in samples 3 and 7. Since the flux corrections were smaller and the specific activity of ^{152}Eu was higher in the INAA irradiation, we used europium/samarium ratios from the INAA irradiation to calculate europium concentrations in Table 4. REE concentrations in Table 4 are used in all subsequent discussion and in all figures.

Table 3. REE in SP and BCR-1. All results, in ppm, are corrected for sample losses during transfers after irradiations. Errors in our data are as in Table 1.

	La	Ce	Nd	Sm	Eu	Gd	Tb	Dy	Tm	Yb	Lu
SP (257.3 μg)											
INAA	45.29 ±.12	81.76 ±.09	34.0 ±1.3	6.048 ±.009	1.059 ±.005		0.6962 ±.0056		0.354 ±.011	2.819 ±.048	0.463 ±.019
RNAA	43.55 ±.14	79.50 ±.15	34.75 ±.79	5.693 ±.006	1.201 ±.007	3.1 ±1.5	0.7472 ±.0022	4.726 ±.026	0.3903 ±.0022	2.599 ±.009	0.4178 ±.0021
Perlman and Asaro (1971)	44.90 ±.45	80.3 ±3.9	35*	5.78 ±.12	1.291 ±.034		0.73*	4.79 ±.19		2.80 ±.36	0.402 ±.036
BCR-1 (185.2 μg)											
INAA	25.08 ±.24	51.65 ±.14	29.7 ±4.2	6.714 ±.023	1.816 ±.008		0.930 ±.011		0.5122 ±.0091	3.98 ±.17	0.634 ±.034
RNAA	23.81 ±.10	53.42 ±.18	30.3 ±1.0	6.844 ±.007	2.181 ±.017		1.124 ±.005	7.451 ±.069	0.6023 ±.0055	3.722 ±.013	0.5724 ±.0050
Nakamura (1974)	24.4 ±.2	54.2 ±.4	28.8 ±.2	6.72 ±.04	1.98 ±.00	6.67 ±.02		6.36 ±.02		3.40 ±.03	0.503 ±.004

*F. Asaro (personal communication).

REFRACTORY ELEMENT FRACTIONATION IN OXIDIZING ENVIRONMENTS

As will be seen in the next section, HAL has huge negative cerium anomalies and other peculiarities in its trace element abundances that suggest formation under highly oxidizing conditions. In trying to explain a much smaller negative cerium anomaly in Allende FUN inclusion C1, Boynton (1978) calculated REE volatilities under the highly oxidizing conditions expected in some types of supernova ejecta. He found that cerium is the most volatile REE under these conditions and proposed that a large fraction of C1 is a supernova condensate. Laboratory-produced volatilization residues made from glasses similar in composition to Allende inclusions show marked negative cerium anomalies (Nagasawa and Onuma, 1979), presumably because cerium has been preferentially volatilized under the oxidizing conditions of the experiment. In order to interpret the chemistry of HAL, we compute in this section the behavior of a large number of refractory trace elements during solid-gas fractionation under oxidizing conditions. We consider processes that may occur in two types of environments: the oxidizing outer shells of supernova ejecta and the oxidizing gas that would result from vaporization of chondritic material into a vacuum. The processes to be considered are kinetically controlled vaporization, equilibrium condensation or vaporization and Rayleigh distillation using equilibrium solid/gas partition coefficients.

Kinetically controlled vaporization of REE

In order to explain HAL's enrichment in the heavy isotopes of calcium and oxygen, Lee *et al.* (1980) proposed that the refractory minerals in HAL formed by volatilization of solid material. They suggested that the cerium anomalies were established during this event because volatilization of silicate and oxide minerals would yield a highly oxidizing gas in which cerium is volatile. There are two ways in which this could have happened. In one, the volatilization process occurred in absence of any gas other than that evolved from the residue. In the other, the volatilization event was so rapid that the evolved gas completely displaced any reducing, hydrogen-rich solar nebular gas. Lee *et al.* (1979) found that loss of half of the calcium in a Rayleigh distillation process would explain the calcium isotope fractionation. Although not explicitly stated, they calculated relative solid/gas partition coefficients for calcium assuming that they fractionated *via* the kinetic isotope effect.

Table 4. RNAA analyses of REE, in ppm, normalized such that La(RNAA) ≡ La(INAA). Europium was calculated from the INAA europium/samarium ratio. Errors are as in Table 1.

Sample	La	Ce	Nd	Sm	Eu	Gd	Tb	Dy	Tm	Yb	Lu
1	13.42 ±.06	<0.13	17.31 ±.80	3.399 ±.008	1.008 ±.018	<6.3	0.312 ±.012	1.554 ±.028	0.049 ±.017	0.306 ±.010	0.0571 ±.0032
2	12.83 ±.06	<0.14	16.57 ±.96	3.615 ±.006	0.967 ±.022	<7.9	0.329 ±.012	1.470 ±.036	0.040 ±.016	0.2425 ±.0098	0.0489 ±.0047
3	4.419 ±.054	0.37 ±.12	11.7 ±1.2	3.266 ±.012	0.686 ±.038	<7.9	0.794 ±.015	6.375 ±.064	0.631 ±.020	3.627 ±.026	0.6413 ±.0061
4	16.65 ±.09	0.39 ±.12	48.3 ±2.0	18.34 ±.02	2.664 ±.026	24.3 ±6.3	4.835 ±.016	38.15 ±.13	3.447 ±.017	21.56 ±.05	4.052 ±.014
7	6.240 ±.036	0.504 ±.059	18.9 ±1.3	6.775 ±.006	1.142 ±.009	12.0 ±3.1	1.978 ±.006	15.31 ±.05	1.456 ±.006	8.951 ±.023	1.816 ±.006

In order to justify the use of these coefficients, one must assume that the calcium mass fractionation takes place by a kinetically controlled process, for example, diffusion of calcium ions or atoms to the surface of the residue or evaporation of calcium atoms from this surface.

It is of interest to consider the effect of kinetically controlled processes on REE. One approach is to treat the REE group as a single element and each REE as an isotope. Without specifying the mass fractionation mechanism, we assumed that it was kinetically controlled. We calculated solid/gas partition coefficients for REE in the standard way for the kinetic isotope effect: they are proportional to the inverse square roots of their atomic weights. Since REE are probably contained in calcium sites and REE are less volatile than calcium, it seems likely that loss of 50% of the calcium in a Rayleigh distillation would lead to loss of much less than 50% of the REE. Evaporation of 50% of the REE yielded a residue preferentially enriched in heavy REE by 10%, with the fractionations a smooth function of atomic weight. Another approach is to assume that mass fractionation takes place during diffusion of REE to the surface of the residue. We assumed that REE diffusion coefficients were inversely proportional to ionic radii, so that solid/gas partition coefficients were inversely proportional to ionic radii. For this case, evaporation of 50% of the REE by Rayleigh distillation yielded a residue with a smoothly fractionated REE pattern, depleted in heavy REE by 10%. Other functional relationships, such as having partition coefficients directly proportional to ionic radii or having logarithms of partition coefficients inversely or directly proportional to ionic radii, also gave smoothly fractionated patterns with depletions or enrichments of $\sim$10% in heavy relative to light REE. None of the above approaches gave large REE fractionations and anomalies in individual REE could not have been produced without those REE having different valences from the others. Under oxidizing conditions, cerium could exist as Ce^{+4}. Since its ionic radius is smaller than those of the trivalent ions of all other REE except lutetium and its charge is different from the most stable charge of all other REE, cerium might diffuse faster and be preferentially lost from the residue. It is unlikely the europium exists as Eu^{+2} under these conditions, so that europium anomalies are not to be expected. It should also be pointed out that such kinetically controlled processes as these would produce exactly the same REE patterns no matter where evaporation takes place, since these processes are not affected by exterior gas composition.

Equilibrium distribution of refractory trace elements

Highly oxidizing gases are found in several shells of supernova ejecta: explosive hydrogen-, helium- and carbon-burning shells with carbon/oxygen < 0.9 and explosive oxygen-burning shells relatively poor in sulfur and silicon (Lattimer *et al.*, 1978). The relative abundances in the hydrogen-burning zone are essentially solar, except that hydrogen has been completely converted to helium. The relative abundances of elements heavier than oxygen in the helium-burning zone are also nearly solar, as long as the temperature is low enough that the release of free neutrons from the reaction $^{22}Ne(\alpha,n)^{25}Mg$ and from the photodisintegration of heavy nuclides like ^{238}U does not take place. Explosive helium-burning does not convert helium to carbon and oxygen very efficiently, but significant burning of ^{14}N can take place. Since nitrogen is an inert gas during condensation under oxidizing conditions, the nitrogen abundance has little effect on condensation sequences. For the purposes of these calculations, we assume the same chemical composition for the hydrogen- and low temperature helium-burning zones of supernova ejecta.

Another way of generating a highly oxidizing gas is by completely evaporating chondritic material. Although such a gas would be similar in relative abundances of condensible elements to hydrogen- and low temperature helium-burning gases, the condensible elements would not be diluted with large amounts of helium, carbon, nitrogen and oxygen, as they are in the latter cases.

Condensation equilibria for a gas having the same composition as C1 chondrites have been calculated by J. M. Lattimer (pers. commun.) at several pressures. The sequence of condensation of refractory phases is similar to that in solar and helium-burning gases.

The method of calculation of lithophile trace element condensation was discussed in detail by Davis and Grossman (1979). The major change in the present calculations is that we now consider condensation of Sr^{+2}, Ba^{+2}, Y^{+3}, Ce^{+4}, Eu^{+2}, Th^{+4}, U^{+3}, U^{+4} and trivalent REE into Ca^{+2} sites of all calcium-bearing condensates rather than only that of perovskite. Sc^{+3}, Zr^{+4}, Hf^{+4}, V^{+2}, V^{+3}, V^{+4}, V^{+5} and Ta^{+5} are permitted to condense into Ti^{+4} sites of all titanium-bearing condensates, including hibonite. The division of trace elements between these two sites was done on the basis of the ionic radii given by Shannon (1976). The host phases of all refractory lithophiles were assumed to be capable of balancing charges of trace elements by substitution of elements of other valences. Since trace element activity coefficients in relevant host phases are not known, ideal solid solution was assumed for all elements. Ionic behavior was also assumed. Application of trace element condensation calculations to HAL is largely concerned with gross comparisons of HAL's composition with calculated trace element patterns in reducing and oxidizing gases. Trace element host phases and condensation sequences are the same in most of the gas compositions that we have considered. Thus, assumption of a reasonable amount of nonideal solid solution behavior would not significantly alter our conclusions based on these comparisons, since the trace element

patterns would be affected nearly equally in reducing and oxidizing gases.

The condensation temperatures of some pure refractory oxide phases were calculated by the method of Grossman (1973). The condensation behavior of refractory siderophile elements was calculated by the method of Palme and Wlotzka (1976). The siderophile elements osmium, rhenium, iridium, ruthenium, iron, platinum, nickel, rhodium, cobalt, palladium and gold were assumed to condense in ideal solid solution in one another. The other two refractory siderophiles, molybdenum and tungsten, have stable gaseous oxide compounds and would be relatively volatile under oxidizing conditions, so they were only included in the solar gas calculation.

Thermodynamic data. Thermodynamic data for REE used in these calculations are slightly different from those used by Davis and Grossman (1979). A consistent set of thermodynamic data for all pertinent species is necessary in order to perform equilibrium calculations as accurately as possible. The free energy functions for gaseous monatomic oxygen, gaseous monatomic REE, gaseous REE monoxides and solid REE sesquioxides were taken from the JANAF Tables (1977), Hultgren *et al.* (1973), Ames *et al.* (1967) and Robie *et al.* (1978), respectively, while Davis and Grossman used values for all of these species given by Ames *et al.* The free energy functions for gaseous europium monoxide of Kordis and Gingerich (1976) were used because plots of the Ames *et al.* free energy functions *vs.* atomic number gave europium anomalies while smooth curves were obtained when the Kordis and Gingerich europium monoxide data were substituted. Zero-degree enthalpies of formation of gaseous monatomic oxygen, gaseous monatomic REE and solid REE sesquioxides were taken from JANAF, Hultgren *et al.* and Robie *et al.*, respectively. These sources for the first two parameters were also used by Davis and Grossman. They obtained values for the latter parameter by extrapolation of higher temperature enthalpy data given by Gschneidner *et al.* (1973). Zero-degree enthalpies of formation for gaseous REE monoxides were taken from Ames *et al.* after correcting for differences between the newer free energy functions and zero-degree enthalpies of formation and those used by Ames *et al.* For 5 gaseous REE monoxides, more recent measurements of zero-degree enthalpies of formation are available: PrO, NdO-Murad (1978); SmO-Hildenbrand (1977); EuO-Murad and Hildenbrand (1976); and YbO-Cosmovici *et al.* (1977). These authors did not give the free energy functions and zero-degree enthalpies of formation of species used in calculating their results from experimental data, but the authors of the first three papers did use their values for these parameters to correct the Ames *et al.* gaseous REE monoxide zero-degree enthalpy data. We compared our recalculations of the Ames *et al.* data with those of the above authors and applied the differences to their new values for zero-degree enthalpies of formation. The zero-degree enthalpy of formation of gaseous ytterbium monoxide was calculated from the dissociation energy of ytterbium monoxide given by Cosmovici *et al.* Since their data were obtained using molecular beams, no corrections for differing free energy functions and zero-degree enthalpies were necessary. From the new and recalculated zero-degree enthalpies of formation and free energy functions, free energies of reactions of the form $Ln_{(g)} + O_{(g)} \rightarrow LnO_{(g)}$ were calculated as a function of temperature. Free energies of reactions of the form $Ln_2O_{3(s)} \rightarrow 2Ln_{(g)} + 3O_{(g)}$ were calculated from free energies of formation of solid REE sesquioxides, gaseous monatomic REE and gaseous monatomic oxygen of Robie *et al.*, Hultgren *et al.* and JANAF, respectively. For siderophile element calculations, required thermodynamic data were calculated from vapor pressures between 1000 and 2000 K given by Hultgren *et al.* Sources of thermodynamic data for other species considered are given in Table 5.

Table 5. Species considered and sources of thermodynamic data.

Element	Gas phase species	Solid phase species
Sr	Sr[1], SrO[2]	SrO[2]
Ba	Ba[1], BaO[2]	BaO[2]
Ce	Ce[3], CeO[4], CeO_2[5]	Ce_2O_3[6], CeO_2[6]
Eu	Eu[3], EuO[4]	EuO[7], Eu_2O_3[7]
Sc, Y, remaining REE	Ln[3], LnO[4]	Ln_2O_3[7]
Th	Th[8], ThO[8], ThO_2[8]	ThO_2[8]
U	U[8], UO[8], UO_2[8], UO_3[8]	UO[8], U_2O_3[8], UO_2[8]
Zr[9]	Zr[10,11], ZrO[10,10], ZrO_2[10,10]	ZrO[10,11]
Hf	Hf[3], HfO[12], HfO_2[13]	HfO_2[7]
V	V[2], VO[2], VO_2[2]	VO[2], V_2O_3[3], VO_2[2], V_2O_5[2]
Ta	Ta[2], TaO[2], TaO_2[2]	Ta_2O_5[2]
Siderophiles	M[3]	M[3]

[1]Chase *et al.* (1974). [2]Chase *et al.* (1975). [3]Hultgren *et al.* (1973). [4]See text. [5]Kordis and Gingerich (1976). [6]Gschneidner *et al.* (1973). [7]Robie *et al.* (1978). [8]Ackermann and Chandrasekharaiah (1975). [9]Free energies were calculated from low temperature enthalpies and free energy functions. The first number for each species gives the data source for the former and the second, the latter. [10]Murad and Hildenbrand (1975). [11]Stull and Prophet (1971). [12]Ackermann and Rauh (1974). [13]Chandrasekharaiah (1967).

Solid/gas distribution coefficients. Corundum is the first major phase predicted to condense from a gas of solar composition, from the oxidizing helium- and carbon-burning shells of supernova ejecta and from a C1 chondritic gas. Hibonite has not been included in any published calculations from this laboratory because thermodynamic data for this phase have only recently become available. When hibonite is included in a solar calculation at 10^{-3} atm total pressure, corundum condenses at 1744 K and reacts with the gas to form hibonite at 1730 K. In calculations with C1 chondritic gas at 10^{-10} to 10^{-14} atm total pressure, hibonite forms by reaction of previously condensed corundum with gas at temperatures 73 to 84° below the corundum condensation temperature (J. M. Lattimer, pers. commun.). Hibonite has not been included in any supernova calculation to date. In helium-burning gas, the calcium/aluminum ratio is the same as that of C1 chondrites and corundum condenses under temperature and pressure conditions intermediate between those of solar and C1 chondritic gases. Thus, the temperature interval between corundum condensation and hibonite formation in helium-burning gas should be intermediate between the intervals in solar and C1 chondritic gases. We assumed that this temperature interval was 50° at all pressures considered for helium-burning gas. Since carbon-burning gas has a calcium/aluminum ratio much lower than that of C1 chondrites, hibonite was not assumed to be stable in this gas. Corundum does not condense in oxygen-burning gas at 10^{-8} atm initial total pressure, so hibonite is not expected to form, either. Since hibonite and corundum have similar thermodynamic stabilities in solar, C1 chondritic and helium-burning gases, uncertainties in thermodynamic data could permit substantial changes in corundum-hibonite transition temperatures or even reversal of the order of condensation of corundum and hibonite. Recent petrographic evidence (Bar-Matthews *et al.*, 1982) suggests that corundum was the first condensate in the solar case, but that it reacted with the gas at slightly lower temperature to form hibonite.

The condensation temperatures of the most refractory pure oxide phases, those of scandium, yttrium, lutetium and zirconium, were calculated for all gas compositions and pressures considered. These phases always condensed at lower temperature than did the most refractory calcium- and titanium-bearing phases, so we assumed that scandium, yttrium, lutetium and zirconium condensed in solid solution in hibonite, melilite and perovskite.

In the first set of calculations, we compare relative solid/gas distribution coefficients, as defined by Boynton (1975), for refractory elements in a gas of solar composition with those for the same elements in one of the most oxidizing gases considered: that generated by complete evaporation of material of C1 chondritic composition. In order to see the effects of gas composition alone, total pressures were chosen such that 5% of the lanthanum was condensed into hibonite, the only condensate phase, at 1723 K in both gases. In the solar case, this occurs at 10^{-3} atm total pressure. J. M. Lattimer (pers. commun.) computed condensation sequences for a nonexpanding C1 chondritic gas at total pressures of 10^{-10}, 10^{-12} and 10^{-14} atm. The total pressure, partial pressure of monatomic oxygen and number of calcium and titanium atoms condensed per liter were extrapolated from the results at the above three pressures to determine the conditions under which 5% lanthanum condensation would occur at 1723 K. The total pressure so obtained was 1.15×10^{-8} atm.

One of the effects of changing gas composition from solar to C1 chondritic is that the major condensate phases become much more refractory. There are two reasons for this effect, both related to the change in chemical composition of the gas. First, in C1 chondritic gas, the condensible elements are not diluted by large amounts of hydrogen and helium, as they are in solar gas. Second, oxygen is bound as H_2O and CO in solar gas, while in C1 chondritic gas, substantial fractions of the total oxygen exist as O and O_2. The substantially higher partial pressure of monatomic oxygen drives condensation reactions toward completion, *e.g.* $Ca_{(g)} + 12AlO_{(g)} + 7O_{(g)} \rightarrow CaAl_{12}O_{19(s)}$ [hibonite]. This is the reason why the pressure in the C1 chondritic gas must be much lower than in the solar gas for 5% condensation of lanthanum to occur at the same temperature in both. In fact, lower pressures are required in all oxidizing gases considered in this work in order to have condensation occur in the same temperature range as in a solar gas.

The results of refractory element condensation calculations in solar and C1 chondritic gases are compared in Fig. 1. The method of eliminating temperature effects also automatically eliminates the effect of composition difference on the solid/gas distribution coefficient for lanthanum. Nevertheless, Fig. 1 is useful in comparing the changes in condensation behavior of other elements relative to lanthanum. The condensation reaction for lanthanum in both solar and oxidizing gases is $LaO_{(g)} + \frac{1}{2}O_{(g)} \rightarrow LaO_{1.5(s)}$ and involves condensation of one half atom of free oxygen per atom of lanthanum condensed. As conditions become more oxidizing, the partial pressure of oxygen will increase, this reaction will be driven to the right and lanthanum will become more refractory. Most of the other REE have condensation reactions of this form, so that there is no change relative to lanthanum in going from solar to C1 chondritic gas. For cerium, the dominant condensation reactions in solar and C1 chondritic gases are $CeO_{2(g)} \rightarrow CeO_{1.5(s)} + \frac{1}{2}O_{(g)}$ and $CeO_{2(g)} \rightarrow CeO_{2(s)}$, respectively. As conditions become more oxidizing, cerium at first becomes more volatile, then is unaffected by increasing partial pressure of oxygen. Since lanthanum becomes more refractory, cerium becomes quite volatile relative to lanthanum in the C1 chondritic gas. Although condensation reactions are different for other elements, similar arguments can

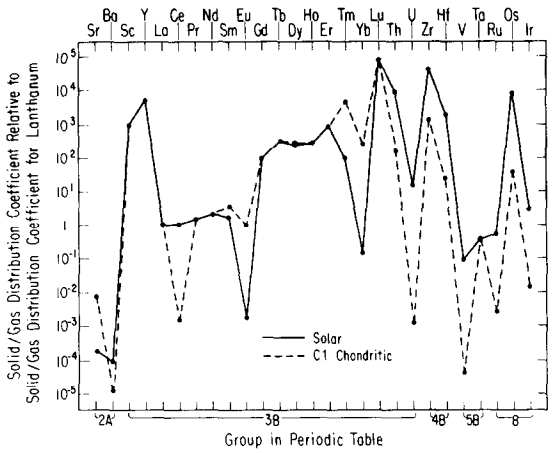

FIG. 1. Solid/gas distribution coefficients for refractory elements relative to that for lanthanum for equilibrium condensation from solar gas at 10^{-3} atm total pressure and 1723 K are compared with those from C1 chondritic gas at 1.15×10^{-8} atm total pressure and the same temperature.

be made. In going from solar to C1 chondritic gas, elements that condense less than one half atom of free oxygen per atom of element condensed will become more volatile relative to lanthanum, while elements that condense more than one half atom of free oxygen per atom of element condensed will become more refractory relative to lanthanum. The refractory siderophiles condense by reactions of the form $M_{(g)} \rightarrow M_{(s)}$, in which oxygen is not involved. Thus, as lanthanum becomes more refractory with increasing partial pressure of oxygen, these elements will become more volatile relative to lanthanum. We have only plotted in Fig. 1 those refractory siderophiles which were determined in HAL. The major changes in condensation behavior in going from solar to C1 chondritic gas are as follows, relative to lanthanum: barium, cerium, thorium, uranium, zirconium, hafnium, vanadium, ruthenium, osmium and iridium become more volatile and strontium, europium, thulium and ytterbium become more refractory. In C1 chondritic gas, strontium, barium, cerium, uranium, vanadium, ruthenium and iridium are the most volatile of the elements determined in HAL which are normally considered to be refractory in a gas of solar composition.

In Fig. 2, we examine the condensation behavior relative to lanthanum for the same elements as in Fig. 1 in a variety of gas compositions at different pressures. For each pressure and gas composition, the calculations were done at two different temperatures, corresponding to 5 and 95% condensation of lanthanum. The cases considered are gas of solar composition under 10^{-3} atm total pressure at 1723 and 1598 K; C1 chondritic gas under 10^{-10} atm total pressure at 1569 and 1474 K, 10^{-12} atm at 1424 and 1348 K and 10^{-14} atm at 1304 and 1241 K; expanding helium-burning gas under 10^{-8} atm initial total pressure at 1452 and 1352 K and 10^{-12} atm at 1228 and 1168 K; expanding carbon-burning gas under 10^{-8} atm at 1588 and 1441 K and 10^{-12} atm at 1320 and 1228 K; and expanding oxygen-burning gas under 10^{-8} atm at 1610 K (5% lanthanum condensation only). Since no attempt was made in this calculation to force the same fraction of the lanthanum to condense at the same temperature in each gas composition, comparing the results at the same total pressure shows the full effects of both temperature and gas composition. Except for the oxygen-burning gas, all of the above cases for oxidizing gases yield relative solid/gas distribution coefficients for a given element that are so similar to one another that they have been plotted together as a single band in Fig. 2, rather than as 14 separate curves. The C1 chondritic and helium- and carbon-burning gases are all about equally oxidizing, so much of the spread of relative distribution coefficients within the band is due to temperature effects. These are due to differences in the temperature dependences of free energies of condensation reactions of different elements. In Fig. 1, it is seen that the heavy REE gadolinium, terbium, dysprosium, holmium, erbium and lutetium have the same distribution coefficients relative to lanthanum in solar and oxidizing gases at the same temperature. In Fig. 2, the band of distribution coefficients for these elements in oxidizing gases lies above that for solar gas. Since all the calculations for oxidizing gases were done at lower temperature than those for solar gas, this shows that the distribution coefficients for these elements increase with decreasing temperature relative to that for lanthanum. The magnitude of this effect is about one order of magnitude for

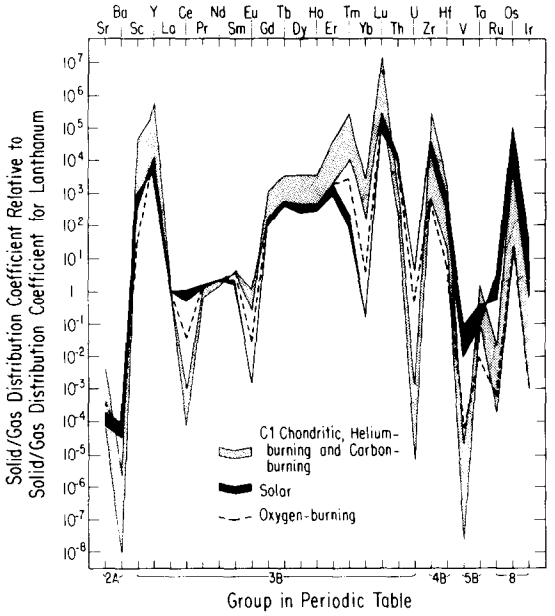

FIG. 2. Solid/gas distribution coefficients for refractory elements relative to that for lanthanum for equilibrium condensation between 5 and 95% condensation of lanthanum. Note that data for a wide range of total pressures for each of the C1 chondritic, helium-burning and carbon-burning gases plot within the band so labelled. For clarity, only the distribution coefficients for 5% lanthanum condensatiion were plotted for oxygen-burning gas. Temperatures and pressures used in these calculations are given in the text.

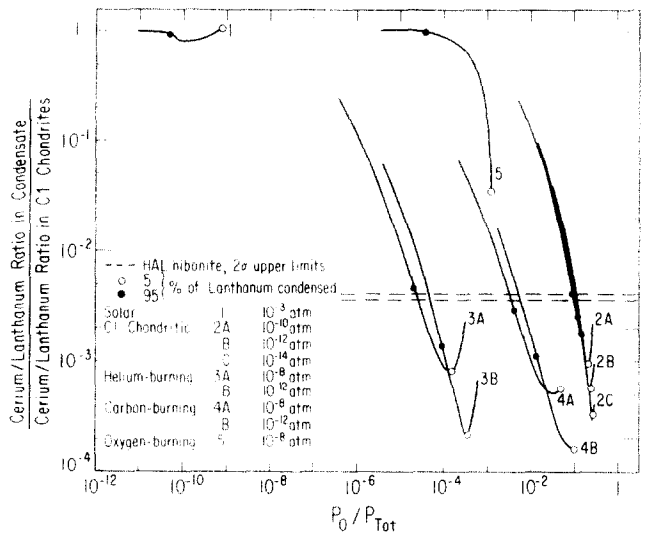

FIG. 3. C1 chondrite-normalized cerium/lanthanum ratios in condensates from all gases considered are plotted as a function of P_O/P_{Tot}. The two horizontal lines give the 2σ upper limits for the two HAL hibonite samples.

each 250°. Similar or smaller effects occur for all other elements considered and the relative distribution coefficients can increase or decrease with temperature. This effect can alter the details of trace element patterns of condensates somewhat, but in all oxidizing gases, strontium, barium, cerium, uranium, vanadium, ruthenium and iridium remain the most volatile of the elements determined in HAL which are normally considered to be refractory in a gas of solar composition. Oxygen-burning gas is significantly less oxidizing than the other oxidizing gases considered.

The most important feature of HAL's trace element pattern is the huge negative cerium anomaly. The sizes of cerium anomalies in condensates were calculated at 10° temperature intervals in all of the gas compositions considered here and the results are plotted as a function of P_O/P_{Tot} in Fig. 3. The latter parameter decreases with falling temperature in all gas compositions due to the stabilization of oxygen-bearing polyatomic molecules. The unusual shape of most of the curves is controlled by two competing effects. In the earliest stage of condensation, the cerium anomaly deepens with falling temperature because, despite the decrease in P_O/P_{Tot}, the solid/gas distribution coefficient of cerium relative to that for lanthanum decreases monotonically. As the temperature falls further, the curves reverse themselves because both cerium and lanthanum become more fully condensed until, in the limiting case of total condensation of both, the anomaly disappears. In any one gas composition, the cerium anomalies become deeper with decreasing pressure. This is due to the fact that, at lower pressure, condensation occurs at lower temperatures where the solid/gas distribution coefficient for cerium relative to that for lanthanum is lower. At the same pressure, carbon-burning gas produces deeper cerium anomalies at higher temperatures than does helium-burning gas. This is because carbon-burning gas is more oxidizing than helium-burning gas. At the same pressure, C1 chondritic gas produces shallower cerium anomalies than does carbon-burning gas, despite higher P_O/P_{Tot} in C1 chondritic gas. This occurs because REE condensation takes place at higher temperature in C1 chondritic gas, outweighing the effect of the higher P_O/P_{Tot}. Cerium anomalies in oxygen-burning gas are smaller than in helium-burning gas at the same total pressure, despite similar P_O/P_{Tot}. This is because REE condensation occurs at considerably higher temperatures in oxygen-burning gas, where the volatilities of lanthanum and cerium are closer together. The reason why the cerium anomaly shrinks more rapidly with P_O/P_{Tot} in the oxygen-burning than in the helium-burning case is that the number of moles per liter of condensed calcium atoms increases more rapidly with falling temperature in the oxygen-burning case, causing all REE to approach total condensation more rapidly. All oxidizing gases except oxygen-burning gas yield condensates with large cerium anomalies over a wide range of REE condensation. Similar diagrams can be constructed to show that strontium, barium, uranium, vanadium, ruthenium and iridium also remain volatile in helium- and carbon-burning gases and C1 chondritic gas over a wide range of pressure and temperature.

Comparison with previous calculations. Our results for the C1 chondritic gas are in agreement with Boynton's (1978) and Boynton and Cunningham's (1981) calculations of refractory lithophile trace element distribution coefficients in oxidizing zones, in that both predict that vanadium, barium, cerium and uranium become more volatile and strontium and ytterbium more refractory relative to lanthanum compared to their behavior in a gas of solar composition. However, there are important differences that cannot be explained by the differences in temperature and gas composition between the two calculations. Boynton predicted that the relative distribution coefficient for cerium

drops by a factor of 30,000 in going to the oxidizing zone, while we predict a factor of only 750. This difference arises because Boynton apparently did not consider solid cerium dioxide, the dominant solid cerium species in oxidizing gases. Boynton calculated that europium and thulium are only slightly more refractory in the oxidizing zone than in the solar case, while we found that the relative distribution coefficients for europium and thulium increase by factors of 570 and 55, respectively. These disagreements are due to the fact that Boynton used the zero-degree enthalpies of formation of Ames *et al.* (1967), which are 21.9 and 9.5 kcal lower, respectively, than those used here. The new values make gaseous europium and thulium monoxides much less stable than gaseous monatomic europium and thulium in the solar case, so that more than one half atom of free oxygen condenses per atom of element condensed and they become more refractory relative to lanthanum with increasing partial pressure of oxygen. Previous calculations by this group (Tanaka *et al.*, 1979), based on the earlier thermodynamic data for gaseous europium monoxide, predicted that europium was considerably less refractory relative to cerium than in our current calculations. The only other major difference between our results and those in the literature is that Boynton and Cunningham predict that the relative distribution coefficient for vanadium drops by a factor of 2,000,000 in going to the oxidizing zone, while we predict a factor of only 2100. The reason for this discrepancy is not known, since Boynton and Cunningham gave neither the source of their thermodynamic data nor the precise gas composition which they used. Other small differences between the calculations can be attributed to differences in temperatures, gas compositions and thermodynamic data.

REE patterns in equilibrium condensates or volatilization residues. We can use the solid/gas distribution coefficients calculated above to compute the REE patterns of solids in equilibrium with gas at various temperatures. We have chosen as an example C1 chondritic gas at a total pressure of 10^{-10} atm. The amounts of minerals condensed were calculated by J. M. Lattimer (pers. commun.). The enrichment factors for REE relative to C1 chondrites were calculated in the solids at each temperature. Plotted in Fig. 4 are REE patterns of condensates at several temperatures. At all temperatures, heavy REE have enrichments that are the same as or greater than those of the light REE. Europium always has about the same enrichment factor as lanthanum and large negative cerium anomalies occur at all temperatures plotted. The maximum enrichment factor for light REE, 31, occurs when they are almost completely condensed, but before forsterite begins to condense. The large amounts of magnesium and silicon that condense at this point substantially dilute the REE. Calculations for helium- and carbon-burning and C1 chondritic gases at a variety of pressures yield similar sequences of REE patterns.

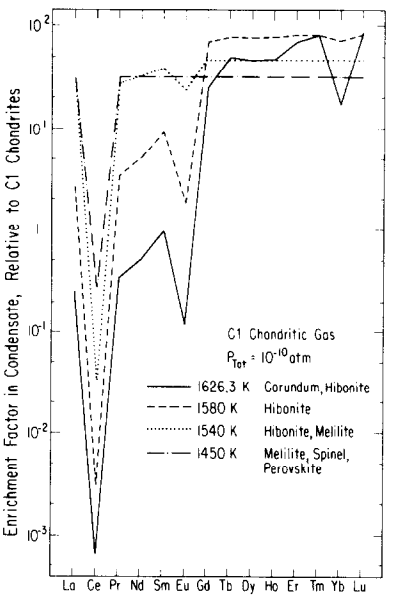

FIG. 4. C1 chondrite-normalized enrichment factors for REE in equilibrium condensates from C1 chondritic gas or in residues from closed system equilibrium vaporization of C1 chondrites at a total pressure of 10^{-10} atm. The mineral names given are the stable solid phases at each temperature.

Thermodynamically controlled vaporization with gas loss

The final fractionation process to be considered is fairly slow vaporization of chondritic material with attendant gas loss. We assume that the process is slow, such that, at all times during the vaporization, there is instantaneous equilibrium between gas and solid. In this case, the fractionation of each element remaining in the solid can be calculated from the Rayleigh equation: $R = (1 - F)^{1/d}$, where R is the fraction of element M remaining in the solid, F is the fraction of solid vaporized and d is the solid/gas distribution coefficient for M. As chondritic material is vaporized, a variety of gases will be evolved: at low temperature, the gas will be sulfur-rich from the decomposition of sulfides; at intermediate temperatures, it will become oxidizing with the breakdown of oxides of iron, magnesium and silicon and release of free oxygen; and at high temperatures, it will remain oxidizing because oxygen will continue to be released when calcium, aluminum and titanium oxides decompose. Thus, vaporization at temperatures high enough to fractionate refractory trace elements is certain to take place under highly oxidizing conditions, providing the only gas in contact with the surface of the residue is that volatilized from it. Calculation of the trace element pattern of a residue made by slow vaporization of chondritic material starting at low temperature is difficult and time-consuming. To demonstrate the nature of the fractionations expected, we have pursued the following model instead: solid material is heated in vacuum initially, but evolves a gas just as oxidizing as C1 chondritic gas, allowing us to use the solid/gas distribution coefficients in Fig. 1. In order to compare this calculation with the closed-system, equilibrium case, we first computed the fraction of each element in the solid at equilibrium in C1 chondritic gas under the same conditions as in Fig. 1: T = 1723 K and $P_{Tot} = 1.15 \times 10^{-8}$ atm. Recall that 5% of the lanthanum is condensed under these conditions. We then used the lan-

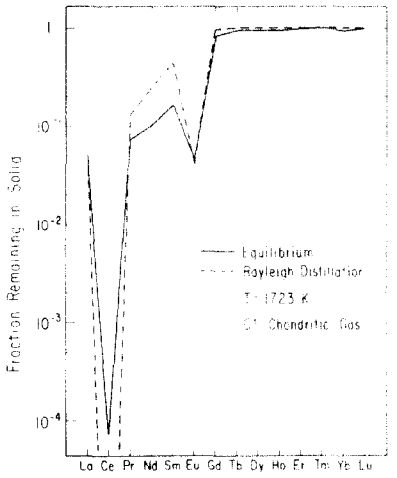

FIG. 5. Comparison of REE pattern produced by closed system equilibrium vaporization with that formed by thermodynamically controlled vaporization with gas loss (Rayleigh distillation) in C1 chondritic gas at 1723 K.

thanum solid/gas distribution coefficient to calculate the fraction of solid that would have to vaporize in a Rayleigh fractionation event such that 5% of the lanthanum remained in the solid following the event. Using this fraction of solid vaporized, 14.6%, and solid/gas distribution coefficients for the remaining REE from Fig. 1, we calculated the fraction of each that would remain in the solid after the vaporization event. The results are plotted in Fig. 5. It can be seen that REE patterns produced by slow vaporization with gas loss resemble those produced by equilibrium condensation or vaporization, but that the degree of fractionation of elements is amplified.

The equilibrium solid/gas partition coefficients for calcium isotopes cannot be calculated because the molecular properties of important calcium-bearing compounds are not known. For this reason, it is not possible to predict the calcium isotopic composition produced by slow vaporization of solid material with gas loss. It is possible that this process could yield fractionations similar in magnitude to those calculated for the kinetic isotope effect (Lee *et al.*, 1979).

ELEMENTAL ABUNDANCES IN SEPARATED PORTIONS OF HAL

Hibonite

The calcium and aluminum contents of the two hibonite samples are very close to the stoichiometric values expected for pure $CaAl_{12}O_{19}$. Although HAL hibonite is purer than any meteoritic hibonite previously studied (Keil and Fuchs, 1971; Grossman, 1975; Allen *et al.*, 1978; Bar-Matthews *et al.*, 1982), it is moderately to strongly enriched in refractory lithophile trace elements (Figs. 6 and 7). The most striking feature of the trace element patterns is the tremendous negative cerium anomaly, best seen in Fig. 7. Although light REE are strongly enriched in HAL hibonite, cerium is undetectable, so that samples 1 and 2 have 2σ lower limits to their C1 chondrite-normalized lanthanum/cerium ratios of 268 and 238, respectively. The only other inclusion known to have a negative cerium anomaly is the FUN inclusion C1 (Conard, 1976), which has a lanthanum/cerium ratio of only 2.91 ± .04 times that of C1 chondrites. Compared to all previously analyzed bulk inclusions or mineral separates from inclusions, HAL hibonite has trace element abundances that are anomalous in many other respects.

In Fig. 6 are plotted refractory element enrichment factors relative to C1 chondrites for the two hibonite samples and, as a comparison, for the mean of nine coarse-grained inclusions (Grossman *et al.*, 1977). It is seen that the latter have uniform enrichments of all refractory elements regardless of geochemical character, a pattern designated as group I by Martin and Mason (1974) and consistent with the interpretation that coarse-grained inclusions represent the solid fraction of an equilibrium high temperature gas-solid fractionation process that took place in a gas of solar composition. It is clear from Fig. 6 that HAL could not have formed in this way. Compared to these inclusions, HAL hibonite is strongly enriched in scandium, lanthanum and neodymium; contains similar levels of samarium, europium, hafnium and tantalum; and is depleted in calcium,

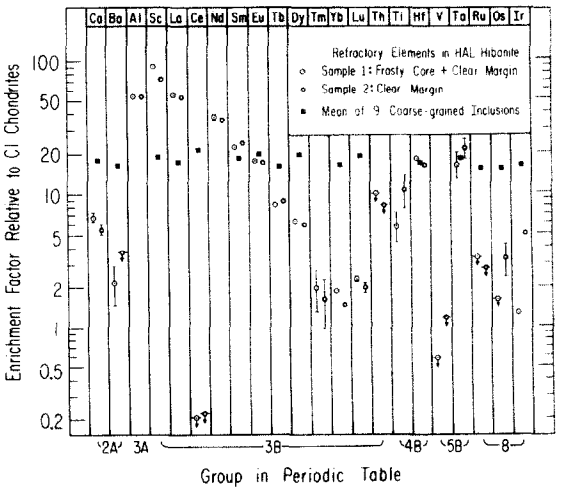

FIG. 6. C1 chondrite-normalized enrichment factors for refractory elements in HAL hibonite, compared with those for the mean of nine coarse-grained Allende inclusions from Grossman *et al.* (1977).

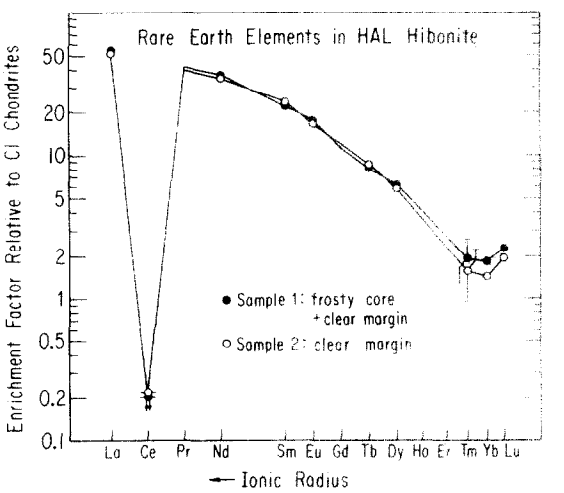

FIG. 7. C1 chondrite-normalized enrichment factors for REE in HAL hibonite. 2σ upper limits to the C1 chondrite-normalized lanthanum/cerium ratios of samples 1 and 2 are 268 and 238, respectively.

barium, ruthenium, osmium, iridium and the remaining REE. Although Grossman *et al.* did not determine thorium and vanadium, HAL hibonite is also depleted in these two elements relative to coarse-grained inclusions. The latter have thorium enrichments of 9.6 to 24.8 compared to C1 chondrites (Tatsumoto *et al.*, 1976; Chen and Tilton, 1976), while samples 1 and 2 have thorium enrichments of <9.8 and <8.0, respectively. HAL hibonite is especially low in vanadium. Samples 1 and 2 have enrichment factors of only <0.6 and <1.2, respectively, while group I inclusions have vanadium enrichments ranging from 3.7 to 25.0 (Conard, 1976; unpublished data from this laboratory). Interestingly, inclusion C1 (Conard) has a vanadium enrichment factor of only 1.06 ± .08. Recall that, of the lithophile elements analyzed which are normally considered to be refractory in a gas of solar composition, strontium, barium, cerium, uranium and vanadium are the most volatile in oxidizing gases (Figs. 1 and 2). Relative to coarse-grained inclusions, HAL hibonite is clearly depleted in barium, cerium and vanadium. Upper limits permit, but do not require, HAL hibonite to be depleted in strontium and uranium.

Although the depletion in heavy REE and the low abundance of refractory siderophiles seen in HAL hibonite are suggestive of the group II refractory element enrichment patterns (Martin and Mason, 1974) seen in many fine-grained Allende inclusions, there are several remarkable features that distinguish the HAL hibonite pattern from those of the group II inclusions. HAL hibonite is considerably richer in scandium than it is in light REE, while the opposite is true in group II inclusions. Group II inclusions have C1 chondritic or lower levels of lutetium and hafnium, while HAL hibonite has C1 chondrite-normalized enrichment factors of 2 and 16 for lutetium and hafnium, respectively. In group II inclusions, tantalum always has about the same enrichment factor as lanthanum, while in HAL hibonite, it has less than half the enrichment factor of lanthanum. The relationship between ionic radius and REE enrichment factor in HAL hibonite is smooth, with the exception of the huge negative cerium anomalies and the upturn of ytterbium and lutetium at the ends of the curves (Fig. 7), while in group II inclusions, this relationship is irregular. HAL hibonite does not have the marked thulium anomaly characteristic of group II inclusions, contrary to our earlier assertion (Tanaka *et al.*, 1979) based on preliminary INAA data. Although HAL hibonite is less enriched in refractory siderophiles than in most refractory lithophiles, it is still enriched in the former relative to group II inclusions and C1 chondrites.

Until now, only one hibonite-rich Allende sample had been analyzed: a mineral separate containing ~70% hibonite, which was hand-picked from a coarse-grained inclusion, CG-11, and analyzed by Davis *et al.* (1978). Like HAL hibonite, the CG-11 sample is especially high in scandium, apparently reflecting the affinity of the hibonite structure for this element. Instead of being strongly depleted in heavy REE like HAL hibonite, the CG-11 sample is moderately enriched in heavy REE relative to light. The low vanadium content of HAL hibonite is apparently not caused by crystallographic exclusion of this element because electron microprobe measurements of CG-11 hibonite (Allen *et al.*, 1978) give vanadium enrichments of 38 to 58 relative to C1 chondrites.

HAL hibonite is remarkable for its extremely low volatile element content. Enrichment factors relative to C1 chondrites for volatile elements in the two hibonite samples are compared with those of coarse-grained inclusions in Fig. 8. As can be seen, the levels of volatile elements in these samples are near or below the lowest levels reported in coarse-grained inclusions, indicating that HAL hibonite was strikingly fractionated from volatile elements during its formation and has been minimally altered since then. Lee *et al.* (1979) and Allen *et al.* (1980) observed thin films of alkali-rich phases, presumably nepheline or sodalite or

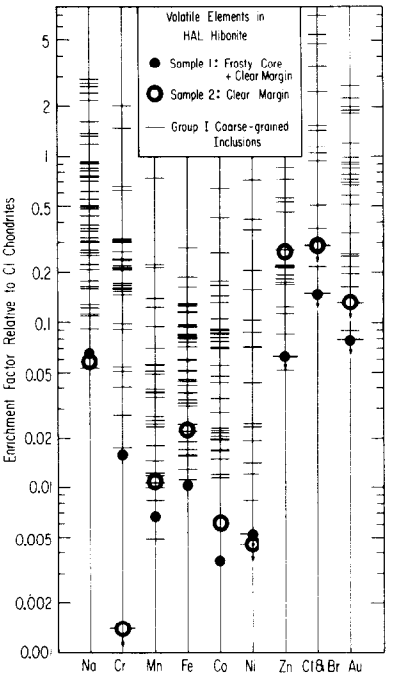

FIG. 8. C1 chondrite-normalized enrichment factors for volatile elements in HAL hibonite, compared with those for coarse-grained Allende inclusions. Data for coarse-grained inclusions were taken from Chou *et al.* (1976), Conard (1976), Davis *et al.* (1978), Grossman and Ganapathy (1975; 1976a), B. Mason (pers. commun.), Mason and Martin (1977), Nagasawa *et al.* (1977), H. Palme (pers. commun.), Palme and Wlotzka (1976), Wänke *et al.* (1974) and unpublished data from this laboratory.

both, on surfaces of HAL hibonite. If all of the sodium in samples 1 and 2 can be attributed to nepheline, these samples contain 0.21 ± .02 and 0.18 ± .07 wt% nepheline, respectively, a very minor amount.

Sample 1 (frosty core plus clear margin) is about 25% higher in scandium and ytterbium than is sample 2 (pure clear margin) and, although the analytical uncertainties are greater, the core also seems to be enriched in thulium and lutetium. There are two possible explanations for this observation. The first is that diffusion of scandium and heavy REE took place during or after exsolution of the titanium-rich needles and that these elements were preferentially taken up by the needles. The second is that hibonite itself is zoned with respect to scandium and heavy REE.

Allen *et al.* (1980) found HAL hibonite to be zoned with respect to iron, with FeO contents increasing from 0.27–0.33 wt% in the frosty core to 0.30–0.42 wt% in the clear margin. Samples 1 and 2 contain 0.24 and 0.54 wt% FeO, respectively, in agreement with the direction of zoning found with the electron microprobe. Our FeO analysis of the clear margin (sample 2) is 0.12–0.24 wt% higher than the electron microprobe analysis. Assuming that the excess iron is due to contamination of sample 2 by black rim, there is 0.5–1.0 wt% black rim present. Sample 2 contains 81 ± 16 ppm zinc, while sample 1 contains <23 ppm zinc. Assuming that all of the zinc in sample 2 is due to contamination by the black rim (which contains 0.66 ± .13 wt% zinc), this sample contains 1.25 ± .35 wt% black rim. Manganese shows an increase of 8.0 ± 4.3 ppm from sample 1 to sample 2, corresponding to 0.69 ± .37 wt% black rim in sample 2. The agreement between these three estimates suggests that sample 2 is contaminated by approximately 1 wt% black rim, an amount that escaped our visual inspection of the sample.

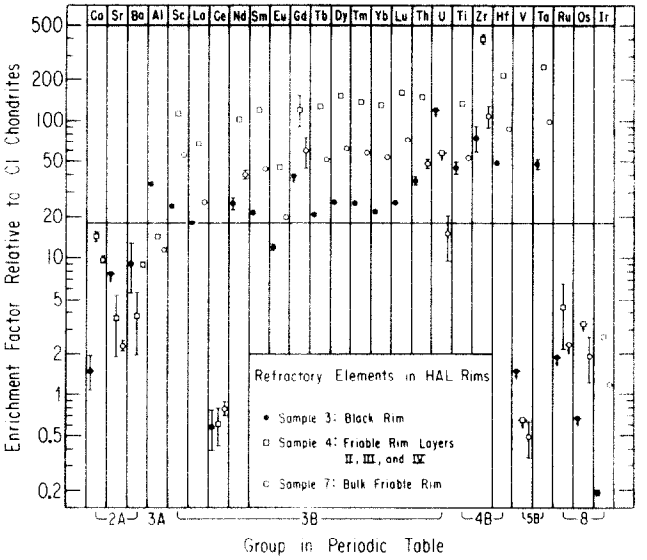

FIG. 9. C1 chondrite-normalized enrichment factors for refractory elements in rim samples from HAL. The horizontal line in the middle of the figure corresponds to the mean enrichment factor for refractory elements in 9 coarse-grained Allende inclusions, 17.5 (Grossman *et al.*, 1977).

Sample 2 is four times higher in refractory siderophiles than sample 1. These elements may have been segregated into tiny nuggets similar to those found previously in coarse-grained inclusions by Wark and Lovering (1976), but Allen *et al.* (1980) found no such nuggets in HAL. The site of refractory platinum metals remains a mystery, although we doubt that these elements are present in the hibonite lattice.

Black rim

Sample 3 is enriched in refractory lithophiles (Fig. 9) with a fractionated enrichment pattern that is strikingly different from that of interior hibonite (Fig. 6). Instead of being strongly enriched in light REE and strongly depleted in heavy REE compared to coarse-grained inclusions, it has levels of light REE that are similar to those of coarse-grained inclusions and it is more enriched in heavy REE (Fig. 10). There is a moderate increase in enrichment factor with decreasing ionic radius, upon which are superimposed large negative cerium and small negative europium anomalies. The V-shaped thulium-ytterbium-lutetium patterns

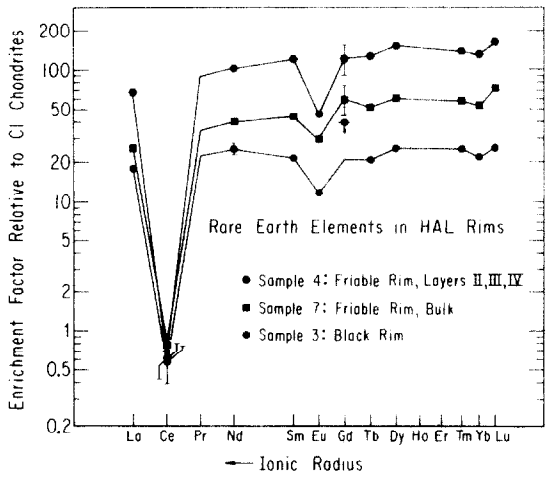

FIG. 10. C1 chondrite-normalized enrichment factors for REE in HAL rim samples.

seen in the hibonite (Fig. 7) are also present here. The C1 chondrite-normalized lanthanum/cerium ratio, 31 ± 10, is not as great as those of the hibonite samples; however, this ratio is not greatly in excess of its 2σ uncertainty and could be much higher, especially considering the large corrections made to the cerium data. The cerium in the black rim may also be real and be due to contamination of HAL by solar material during alteration. The black rim is higher in scandium, titanium, zirconium, hafnium, tantalum and thorium than are coarse-grained inclusions. It has extremely low levels of refractory siderophiles and, like the hibonite, is low in vanadium and barium. Compared to coarse-grained inclusions, it is also low in strontium and might also be low in uranium.

Bulk chemical analyses of the black rim by electron microprobe (Allen *et al.*, 1980) and INAA (this work) are compared in Table 6. There is good agreement between the analyses for most elements, but our data for MgO and FeO are much higher and much lower, respectively, than those of Allen *et al.* In order to compare the composition of aluminum iron oxide in our sample with that inferred by Allen *et al.*, we corrected for the presence of all other phases possibly present. If we assume that sodalite in sample 3 has the same chlorine/bromine ratio as C1 chondrites, 214 (Dreibus *et al.*, 1979), sample 3 contains <0.21 wt% so-

Table 6. Chemical analyses of the black rim (in wt%). Electron microprobe data are summaries of eight wavelength dispersive analyses (J. M. Allen, personal communication). Errors in INAA data are as in Table 1.

	INAA	Electron microprobe Range	Mean
Na_2O	2.371 ± .076	1.88 - 3.75	2.30 ± .61
MgO	11.7 ± 4.1	0.15 - 0.38	0.26 ± .08
Al_2O_3	58.14 ± .85	50.32 - 60.00	55.98 ± 3.45
SiO_2	10.3 ± 4.2	5.69 - 18.23	9.80 ± 4.67
CaO	2.06 ± .60	1.86 - 5.37	3.02 ± 1.29
Sc_2O_3	0.02282 ± .00002	<0.03 - 0.06	
TiO_2	2.82 ± .38	0.36 - 1.18	0.82 ± .34
V_2O_3	<0.011	<0.02	
Cr_2O_3	0.00602 ± .00016	<0.02 - 0.03	
MnO	0.1493 ± .0043	0.11 - 0.16*	0.14 ± .02*
FeO	11.27 ± .03	19.16 - 31.76	27.26 ± 4.60
ZrO_2	0.0313 ± .0069	<0.03 - 0.04	

*Based on six analyses.

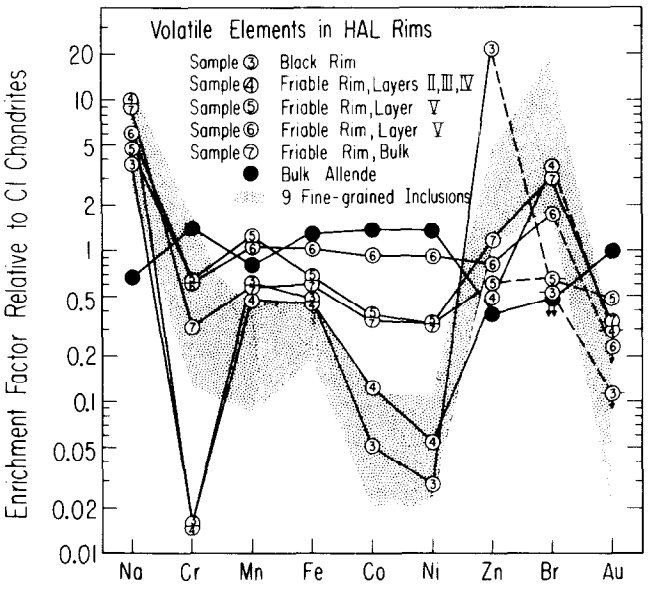

FIG. 11. CI chondrite-normalized enrichment factors for volatile elements in HAL rim samples. The shaded region represents the range of volatile element enrichments found in 9 fine-grained Allende inclusions analyzed by Grossman and Ganapathy (1975; 1976b). The data for bulk Allende were taken from Jarosewich and Clarke (1980).

dalite. Using the sodium and titanium contents, we calculate that 10.87 ± .35 wt% nepheline and 4.80 ± .65 wt% perovskite are present. After correcting the bulk analysis for the presence of these phases, 0.08 ± .66 wt% CaO and 5.7 ± 4.2 wt% SiO_2 remain. The low CaO indicates that sample 3 contains little anorthite, the only remaining SiO_2-bearing phase, so SiO_2 must be at the low end of the quoted range. SiO_2 is determined by difference, so that its uncertainty is dominated by the uncertainty in MgO. If SiO_2 is at the low end of its range of uncertainty, MgO must be at the high end of its range. Using the corrected bulk analysis, we calculate that aluminum iron oxide in sample 3 has a molar $Al_2O_3/(Al_2O_3 + MgO + FeO)$ ratio of 0.543 ± .057 which is in good agreement with the range, 0.49–0.69, and mean, 0.55, inferred by Allen *et al.* The molar MgO/FeO ratio is 1.85 ± .65, far greater than the ratios calculated from the Allen *et al.* analyses, 0.012–0.018 in the black rim and 0.43–0.53 in friable rim layer II. It is unlikely that the high magnesium content of sample 3 could be caused by contamination from an adjacent layer, since interior hibonite contains no detectable magnesium and friable rim layer I contains no magnesium-bearing minerals. It appears from our analysis that the aluminum iron oxide phase can be far more magnesium-rich than even the variety found by Allen *et al.* in the friable rim.

Volatile element contents of the black rim are generally below those of C1 chondrites, but not nearly as low as those of hibonite. The volatile element enrichment patterns of HAL samples are compared with those of fine-grained Allende inclusions (Grossman and Ganapathy, 1975; 1976b; unpublished data from this laboratory) in Fig. 11. The pattern for the black rim resembles those of fine-grained inclusions with three important differences: the black rim is much higher in zinc and much lower in chromium and bromine. Zinc is enriched in the black rim by a factor of 21.5 ± 4.3 relative to C1 chondrites. High levels of zinc are occasionally found in spinels near or within altered regions of coarse-grained inclusions and in terrestrial spinels. Conard (1976) found unusually high levels of zinc in a bulk sample of inclusion C1 and Wark and Wasserburg (1980) found zinc-rich spinels in altered regions of C1. Zinc may have entered the black rim during the alteration event when nepheline was deposited. Another possibility is that zinc-rich spinel was present in the assemblage which melted to form the glass that later devitrified to give the present black rim, although it is curious that chromium, another moderately volatile element with an affinity for spinel, is absent. The physical and chemical conditions under which moderately volatile elements condensed in the black rim differed from those under which these elements condensed in fine-grained inclusions. The C1 chondrite-normalized sodium/cesium ratio of the black rim, 3.1 ± 1.1, is in agreement with the range found in fine-grained inclusions, 3.2 to >8.7 (unpublished data from this laboratory).

Friable rim

Sample 4. Allen *et al.* (1980) estimated that rim layer III contains 85% calcium phosphate and 10% perovskite by volume, corresponding to 83 and 12% by weight, respectively. Although we intended that it contain only rim layer III, sample 4 must contain material from adjacent rim layers, because the total calcium content corresponds to only 35 wt% calcium phosphate. The high titanium content, corresponding to 18.35 ± .44 wt% perovskite, and the high sodium content, corresponding to 31.30 ± .55 wt% nepheline, indicate that portions of adjacent perovskite- and nepheline-rich rim layers II or IV of both are included in this sample. Assuming that all remaining calcium is in calcium phosphate, we calculate that sample 4 contains 21.9 ± 3.0 wt% calcium phosphate, or 26 wt% rim layer III. This calcium phosphate content must be regarded as an upper limit, since other calcium-bearing minerals from rim layers II and IV must also be present. The exact amounts of additional minerals present in sample 4 cannot be calculated, because the number of phases possibly present exceeds the number of elements determined. A substantial amount of aluminum iron oxide and andradite must be present to account for the high iron content.

The refractory element and REE enrichment patterns of sample 4 are shown in Figs. 9 and 10. The patterns closely resemble those of the black rim, except that enrichment factors are considerably higher. The C1 chondrite-normalized lanthanum/cerium ratio is 43 ± 13, but could be higher for the same reason mentioned for sample 3. This sample is higher in refractory siderophiles than are the other friable

rim samples, but the levels are still only 2 to 4 times those of C1 chondrites. The sample is also low in uranium compared to other refractories. It can be inferred that FUN inclusion C1 is also low in uranium. Chen and Wasserburg (1981) calculated the thorium/uranium ratio of C1 from its lead isotopic composition and found a very high ratio compared to C1 chondrites and to other coarse-grained Allende inclusions. If C1 is not greatly enriched in thorium compared to other refractory elements, it must be strongly depleted in uranium. Sample 4 is the only one with counting statistics sufficient to distinguish its zirconium/hafnium ratio, 52.4 ± 4.2, from that of C1 chondrites, 28.2 (Ganapathy *et al.*, 1976). Zirconium/hafnium fractionations are extremely rare in nature (Shima, 1979) and it is of interest to consider whether this phenomenon might be due to the unusually oxidizing conditions under which HAL formed. Referring to Fig. 1, it is seen that zirconium is considerably more refractory than hafnium in both solar and oxidizing gases; however, these elements both become more volatile under oxidizing conditions. Thus, separation of zirconium from hafnium can occur at lower temperatures in oxidizing gases. This means that more potential host phases may have condensed, which may allow greater opportunity for fractionation.

The volatile element enrichment pattern of sample 4 is shown in Fig. 11. The pattern resembles that of the black rim, but has much lower zinc and much higher bromine enrichments. With the exception of chromium, the pattern also closely resembles those of fine-grained inclusions.

Samples 5 and 6. These samples are similar to one another in bulk composition, with sample 6 being somewhat higher in iron and the siderophiles cobalt and nickel. From their bromine, sodium and titanium contents, samples 5 and 6 contain <0.6 and 1.6 wt% sodalite, 14.9 and 17.1 wt% nepheline and 2.9 and <0.7 wt% perovskite, respectively.

Refractory element abundances in samples 5 and 6 are low, at or below C1 chondrite levels for most elements. This is unusual, since the refractory major elements calcium and aluminum are enriched relative to levels in C1 chondrites by factors of 7 to 17. If the calcium- and aluminum-bearing minerals in rim layer V were high-temperature condensates, they would be expected to be considerably higher in refractory trace elements. This would also be expected if those phases formed by secondary alteration of more refractory minerals.

The volatile element enrichment patterns of samples 5 and 6 are shown in Fig. 11. Rim layer V is substantially higher in chromium than are the inner friable rim layers, indicating that layer V contains a component not found in the inner rim layers. The fact that chromium, iron, cobalt and nickel concentrations of samples 5 and 6 are intermediate between those of the inner friable rim layers and bulk Allende suggests that this additional component is Allende matrix. It is not possible to duplicate the volatile element patterns of samples 5 and 6 by simply mixing bulk Allende with inner rim material. This failure stems from our lack of knowledge of the precise composition of Allende matrix and the material to which Allende matrix was added to form rim layer V. Furthermore, petrographic evidence shows that components were added to the friable rim layers following their accretion. Qualitatively, however, the chemical data show that a component similar in composition to bulk Allende is present in rim layer V. This supports the proposal of Allen *et al.* (1980) that rim layer V contains mineral grains identical to those found in the Allende matrix.

Sample 7. This sample has a bulk composition that is intermediate between those of sample 4 and samples 5 and 6, as expected for a bulk friable rim sample. From the bromine, sodium and titanium contents of sample 7, we calculate that it contains 2.4 wt% sodalite, 25.3 wt% nepheline and 7.3 wt% perovskite.

The refractory element and REE enrichment patterns of sample 7 (Figs. 9 and 10) are similar to, but show lower enrichment factors than, sample 4, as expected for a mixture of refractory element-rich and refractory element-poor rim layers. Sample 7 has a C1 chondrite-normalized lanthanum/cerium ratio of 32.2 ± 3.8. The detectable cerium is probably due to contamination of HAL by solar material during late stage alteration. The volatile element enrichment pattern (Fig. 11) of sample 7 is intermediate between those of samples 4 and 6, as expected for a bulk rim sample.

Refractory lithophile trace element components in rims

HAL rim samples 3, 4 and 7 have very similar trace element and REE enrichment patterns. In these samples, measured concentrations of all refractory lithophile trace elements except strontium, barium, cerium, uranium and vanadium increase linearly with calcium and titanium content in the order 3 to 7 to 4. Since sample 7 is a bulk friable rim sample and sample 4 contains only friable rim layers II, III and IV, the host phases for refractory lithophile trace elements must be concentrated in layers II, III and IV. There are a number of potential host phases in these layers. Major phases known to accept REE and other refractory lithophiles include perovskite, calcium phosphate and grossular. The trace phases titanium scandium zirconium oxide, titanium iron oxide and aluminum iron oxide may also take up substantial amounts of these elements. Although likely host phases for refractory lithophiles were not found in the black rim (Allen *et al.*, 1980), it is possible that they were present in a precursor assemblage that was later melted to form the black rim. The only significance of the correlations between refractory lithophiles is that the components containing them are diluted to various degrees by other phases in the rim samples selected for analysis.

ORIGIN OF HAL

Existing models

Two classes of models have been proposed to explain the various properties of HAL. The first, proposed by Lee *et al.* (1979; 1980) to explain mass fractionated calcium and oxygen isotopes, is that HAL is a volatilization residue that has back-reacted with more normal solar material. The second, proposed by Allen *et al.* (1980) and driven by textures in HAL, is that HAL formed by accretion of grains that condensed in an isotopically anomalous region.

Lee *et al.* (1979) measured magnesium and calcium isotopic compositions in the hibonite, black rim and friable rim of HAL. They found magnesium to be isotopically normal in all samples, with concentrations increasing from near blank levels in the hibonite to fairly high levels in the friable rim. They found calcium to be of uniform isotopic composition in all samples: it is mass fractionated, favoring the heavy isotopes, and has small non-linear anomalies of nuclear origin. This isotopic evidence, combined with petrographic evidence available at that time, led Lee *et al.* to suggest that HAL hibonite formed from a volatilization residue from which 50% of the calcium and all of the magnesium had been evaporated. The starting material for this residue was believed to have contained exotic nuclides from a special nuclear source, which gave rise to the small non-linear anomalies in calcium. They proposed that the black and friable rims formed by alteration of the residue at low temperature, introducing isotopically normal magnesium, but no calcium.

Allen *et al.* (1980) performed a detailed study of the mineralogy and petrography of HAL and concluded that the black and friable rims could not have formed by alteration of a volatilization residue. They found that the hibonite had reacted partially with a melt that quenched to form the black rim. They proposed that the friable rim attained its sedimentary texture by accretion of condensate grains, although they could not reconcile the sequence of layers with condensation from a simple monotonically cooled gas. To explain the variety of grains in the friable rim, different physical and chemical histories seem to be required for each layer. The alkali-rich minerals nepheline and sodalite could have formed by gas phase alteration of previously accreted condensate grains. While present in only trace amounts in the core, they are the most abundant minerals in some friable rim layers. To explain the isotopic composition and the substantial amount of oxidized iron in refractory minerals, Allen *et al.* proposed that most of HAL formed in a reservoir that was isotopically and chemically distinct from solar composition.

Lee *et al.* (1980) measured the oxygen isotopic composition of HAL and found that hibonite is mass fractionated in favor of the heavy isotopes relative to spinel in most Allende coarse-grained inclusions, whereas the oxygen isotopic compositions of the two friable rim samples are similar to those of melilite and alkali-rich alteration products in all inclusions. The black rim is similar in composition to the friable rim, but slightly displaced towards hibonite. Lee *et al.* cited these results as providing further support for the volatilization model, since a volatilization residue should be enriched in the heavy isotopes of oxygen. They proposed that a mass fractionated residue, perhaps formed by evaporation of interstellar grains, back-reacted with more normal material to explain the fairly normal isotopic composition of the friable rim. They noted that the samples that were most completely exchanged had the largest amounts of alkali-rich alteration minerals. In the model of Allen *et al.* (1980), the oxygen isotopic composition of HAL hibonite would be postulated to be characteristic of the exotic reservoir in which it condensed. The normal oxygen in the friable rim would indicate that alteration of HAL took place in the same reservoir as that in which all other Allende inclusions were altered.

Conclusions based on trace element abundances

The most unusual feature of all HAL samples is their depletion, relative to other refractory trace elements, in strontium, barium, cerium, uranium and vanadium (Figs. 6 and 9). These five elements exhibit a wide range of geochemical properties, but have in common the trait that, of the lithophile elements determined which are normally considered to be refractory in a gas of solar composition, they are the most volatile in an oxidizing gas. This implies that HAL experienced a high temperature gas-solid fractionation event under extremely oxidizing conditions. The presence of oxidized iron in refractory element-bearing minerals suggests that these conditions allowed oxidized iron to condense at high temperatures, although it is possible that iron was introduced during later alteration.

All HAL samples are depleted in osmium, iridium and ruthenium. Ruthenium and iridium are less refractory in oxidizing gases than the refractory lithophiles and, as a result, may have been excluded from HAL at the temperature at which it was chemically isolated from the gas. Osmium, however, is more refractory than many of the refractory lithophiles. If HAL formed by condensation, the silicates and oxides must not have served as heterogeneous nucleation sites for osmium. Furthermore, metallic osmium may have failed to nucleate homogeneously. Support for this suggestion comes from the fact that osmium is not nearly as supersaturated at lithophile element condensation temperatures in oxidizing gases as it is in solar gas. Alternatively, a refractory siderophile element-rich phase may have nucleated homogeneously but simply failed to accrete with other HAL phases. If HAL formed as a volatilization residue, osmium and other trace siderophiles may have been lost by carrier distillation with more abundant, less refractory siderophiles, an idea suggested by Notsu *et al.* (1978) to explain premature iridium loss from laboratory-produced evaporation residues. Another possibility might be evaporative loss of these elements as volatile halides or oxyhalides.

There are two major refractory lithophile element-bearing components in HAL. The first controls refractory lithophile trace element abundances in rims. It has a REE pattern (Fig. 10) which is characterized by a deep negative cerium anomaly, moderately increasing enrichments from lanthanum to samarium, a small negative europium anomaly and fairly uniform enrichments of heavy REE and which closely resembles that calculated for an equilibrium condensate or residue from a highly oxidizing gas (Fig. 4). This pattern could be produced by (1) condensation from the gas generated by total vaporization of chondritic material, (2) partial equilibrium vaporization of chondritic material in absence of any gas other than that generated by the vaporization, (3) thermodynamically controlled partial vaporization with gas loss, or (4) equilibrium condensation in the oxidizing gases found in supernova ejecta. In all of these situations, solids will be depleted in strontium, barium, cerium, uranium and vanadium relative to other refractory lithophile elements. The second major refractory element-bearing component, hibonite, has a strongly fractionated REE pattern, with a 20-fold decrease in enrichment factor from lanthanum to lutetium that is a smooth function of ionic radius, upon which is superimposed a huge negative cerium anomaly. Strongly fractionated REE patterns are easily produced in high temperature solid-gas fractionation, but the fractionations are by

Table 7. Refractory lithophile element enrichment factors in bulk HAL, relative to C1 chondrites.

Element	Enrichment factor	Element	Enrichment factor
Sc	81.4	Dy	82.1
La	49.5	Tm	93.8
Ce	0.4	Yb	69.3
Nd	64.2	Lu	86.2
Sm	68.9	Zr	196.0
Eu	29.2	Hf	110.8
Tb	69.2	Ta	130.5

no means a smooth function of ionic radius (Boynton, 1975; Davis and Grossman, 1979). For a solid having the lanthanum/lutetium ratio of HAL hibonite and generated by solid-gas fractionation under equilibrium conditions or by thermodynamically controlled vaporization with gas loss, the smooth fractionations of lanthanum, neodymium, samarium and europium from one another observed in the hibonite would not be expected in any of the oxidizing gases considered. Kinetically controlled vaporization is not capable of producing fractionations of the magnitude seen in HAL hibonite. The only other reasonable means of producing this fractionation is partitioning of REE between hibonite and some other components.

The components with which hibonite partitioned REE are probably those in the rims, since both hibonite and the rims have negative cerium anomalies, the V-shaped thulium-ytterbium-lutetium pattern and the same calcium isotopic anomalies. Such partitioning cannot be ruled out, since there is such a wide variety of potential REE host phases in the rims, some of which favor light REE, some intermediate REE and some heavy REE relative to melts, and many of which have unknown REE partitioning behavior.

When partitioning of REE is observed between two components, it is usually concluded that it results from an igneous event in which both components participated. Detailed petrographic study (Allen *et al.*, 1980) shows, however, that the hibonite and friable rim of HAL are not related to one another through an igneous event. Rather, the friable rim seems to be a sedimentary deposit of grains about the hibonite and black rim. Could REE partitioning have occurred during a sintering process that failed to erase the sedimentary texture? In order for negative europium anomalies to be produced in the rim during such an event, conditions must have been reducing enough for Eu^{+2} to form, so that it could partition differently from its trivalent neighbors. Since all other evidence indicates that HAL experienced oxidizing conditions throughout its history, it is unlikely that REE were redistributed by sintering. One possibility that cannot be excluded is that hibonite and another condensate that was later incorporated into the rim coexisted as individual grains in a hot gas, such that REE were partitioned between them without physical contact between them. Examining Fig. 4, we see that a negative europium anomaly could occur in the rim component alone if it were removed from the gas at a slightly higher temperature than was hibonite.

The REE seem to have condensed into both hibonite and the rim component, so that refractory element enrichment patterns of the individual components should not be directly compared with calculated patterns of bulk condensates or residues. We can compute the bulk refractory element enrichment pattern for HAL from estimates of relative amounts of hibonite, black rim and friable rim layers. We assume that HAL is spherically symmetric, with hibonite having a radius of 500 μm and the rim layers having the thicknesses shown in Fig. 6 of Allen *et al.* (1980). Rim layer V was not included in this calculation. This layer contains negligible concentrations of refractory lithophile trace elements, so that including it would lower absolute concentrations, but would not affect relative abundances. We assume that sample 4 is a representative sample of rim layers II, III and IV. Since rim layer I contains no perovskite, we assume that it contains no refractory trace elements. Under these assumptions, the bulk composition of HAL can be calculated by adding 22.7% hibonite, 16.5% black rim and 50.2% sample 4. The resulting trace element enrichment factors for this bulk composition are shown in Table 7.

The REE pattern for bulk HAL is similar to that of sample 4, since the bulk is dominated by the rim. It closely resembles that of an equilibrium condensate or residue from C1 chondritic gas at 10^{-10} atm and 1540 K (Fig. 4). The partitioning of REE between hibonite and the rim clearly demonstrates that our assumption of ideal solid solution of all trace elements into all relevant host phases is incorrect. At the temperature at which the REE pattern of condensate most closely matches that of bulk HAL, REE host phases include hibonite, melilite and perovskite. A wide range of assumptions of reasonable amounts of nonideality in condensate host phases is possible, but the effect of these would only be a slight change to the temperature at which the best match between the calculated and observed REE patterns is obtained. There are features of the refractory element enrichment pattern of bulk HAL that lead us to believe that it does not represent the total condensate. In bulk HAL, zirconium, hafnium and tantalum all have enrichment factors that are greater than that of lutetium; yet, not all of them are more refractory than lutetium (Figs. 1 and 2). In fact, in oxidizing gases, they are all less refractory than lutetium, assuming ideal solid solution. There is nothing peculiar about these three elements that would cause them to be enriched relative to REE during nucleosynthesis. The one thing that they do have in common is that their ionic radii are the smallest of all elements that are refractory in oxidizing gases (Shannon, 1976). The enhanced enrichment of these three elements at first suggests that the above estimates of the relative proportions of refractory element-bearing components in HAL may be incorrect; however, it turns out that no combination of the two refractory

lithophile element-bearing components will yield a pattern that is uniformly enriched in all refractory elements. If HAL condensed from a gas with refractory elements initially in C1 chondritic relative proportions, it must not have sampled all of the refractory element-bearing components. Specifically, it is missing or contains only minor amounts of a REE-rich and relatively zirconium-, hafnium- and tantalum-poor component. Of the most refractory minerals to form in oxidizing gases, melilite is missing from HAL. One interesting feature of melilite is that it has calcium sites into which REE can substitute, but no sites appropriate in size for elements with small ionic radii, such as titanium, zirconium, hafnium and tantalum. Thus, melilite fits the description of the refractory element-bearing component that is postulated to be missing from HAL. Melilite has a slight tendency to take up light REE relative to heavy, judging from melilite-liquid partitioning experiments (Nagasawa *et al.*, 1980). If melilite favors light relative to heavy REE compared to the combination of all other condensate phases, its absence from HAL could contribute to the observed depletion in light REE.

Major and trace element abundances place some constraints on the mechanism and location of the gas-solid fractionation event. The processes of thermodynamically controlled vaporization with gas loss and kinetically controlled vaporization can produce oxidizing environments anywhere, since the original solids provide their own oxidizing gas. Kinetically controlled vaporization is not a viable process, however, because it is not capable of producing europium anomalies under the oxidizing conditions known to have existed at the time of the gas-solid fractionation event. Recall that petrographic work shows that the hibonite and friable rim layers did not form in contact with one another. Because of this, hibonite and REE-bearing components in the friable rim could not have communicated chemically with one another in a kinetically controlled vaporization event, as gas is completely removed from the system as soon as it evaporates from the surface of the residue. Thus, the observed distribution of REE between hibonite and friable rim could not have been produced in such a process.

The chemical composition of the solid produced in an equilibrium condensation or vaporization process depends on the chemical composition of the gas with which the solid equilibrated. If HAL formed by one of these processes, the reservoir in which the equilibration took place can be restricted on the basis of HAL's chemical composition. Equilibrium condensation or vaporization in the oxygen-burning zone of supernova ejecta is not permissible, because conditions are not oxidizing enough to produce cerium and vanadium anomalies of the magnitude seen in HAL. In the carbon-burning zone of supernova ejecta, the relative abundances of the light elements are very different from solar abundances, but heavy elements should have relative abundances similar to solar ones, because the processes of light element nucleosynthesis have relatively little effect on heavy elements. It is therefore reasonable to assume that the lanthanum/titanium ratio in this zone is about the same as that of C1 chondrites. From the titanium/aluminum ratio of the carbon-burning zone given by Lattimer and Grossman (1978), we calculate that this zone should have a lanthanum/aluminum ratio of 0.02 times that of C1 chondrites. The C1 chondrite-normalized lanthanum/aluminum ratios in samples 1, 2, 3, 4 and 7 are 1.02, 0.97, 0.52, 4.78 and 2.24, respectively, far from the ratio expected in the carbon-burning zone. Since gross fractionation of lanthanum from aluminum could have taken place between HAL and its parent reservoir, this is not a conclusive argument for ruling out formation of HAL by equilibrium condensation or vaporization in a carbon-burning zone; however, it does make such an origin unlikely. Similar arguments against such an origin in an oxygen-burning zone can also be constructed, but we have already ruled out this scenario on other grounds, above. We can thus restrict the location of equilibrium condensation or vaporization processes to the hydrogen- or helium-burning zones of supernova ejecta or to a region enriched in the evaporation products of material with near-chondritic relative abundances of refractory elements. All of these gases are sufficiently oxidizing to produce the observed cerium and vanadium anomalies.

Recall that the site of fractionation by thermodynamically controlled vaporization with gas loss cannot be restricted because the grains provide their own oxidizing atmosphere. As discussed above, however, the constituents of HAL all have near-chondritic ratios of light to heavy refractory elements, a feature which would not be expected in the oxygen- or carbon-burning zones of supernova ejecta. Thus, although we cannot rule out vaporization in such zones, the original grains could not have formed therein.

General conclusions

No features of the trace element abundance patterns in HAL by themselves rule out the model of Lee *et al.* (1979; 1980) for formation of HAL by Rayleigh fractionation during evaporation. The model requires an oxidizing gas adjacent to the grain surfaces during evaporation. The rate of gas evolution must be great enough that the gas released at the surface can completely displace any surrounding, reducing, hydrogen-rich solar gas. Furthermore, this process must continue for long enough that, despite gas dissipation, an oxidizing environment is maintained in the vicinity of the residue for long enough that cerium and other volatile elements can diffuse to the surface and evaporate in response to the composition of the gas. The most probable site for satisfying these constraints may be the center of a large region in which the ratio of interstellar dust to am-

bient gas had been enriched prior to vaporization. The model does encounter difficulty in reconciling the isotopic, trace element and mineralogical data. We have seen that the different europium/samarium ratios of hibonite and the rim component imply removal of these components from equilibrium with the gas at different temperatures. Furthermore, Allen *et al.* (1980) saw in the rims a large number of calcium-bearing phases that exhibit a wide range of thermal stabilities relative to hibonite in cosmic gases. Heated to some high temperature, they would presumably vaporize to different degrees in the same length of time. Rims and hibonite, however, have identical calcium isotopic compositions. Thus, if all of these calcium-bearing phases are volatilization residues, the Lee *et al.* model would require the fortuitous coincidence that the assemblage of calcium-bearing phases in the rims has a combination of calcium isotope gas-solid partition coefficient and degree of vaporization that produces the same calcium isotopic mass fractionation as the hibonite. If, however, the rim is an alteration product of a hibonite-bearing residue, as suggested by Lee *et al.*, an alternative possibility is that the diversity of calcium-rich rim phases was produced during the alteration process, as long as no calcium was added at that time. But it is likely that REE in rims are largely contained in a calcium-bearing component. This component could not have formed in an alteration process, as the partitioning of europium between it and core hibonite indicates that it was removed from equilibrium with the gas at a higher temperature than was hibonite.

Allen *et al.* (1980) proposed that HAL is an aggregate of condensate grains from a chemically and isotopically exotic reservoir. One advantage of a ready-made, mass fractionated reservoir is that all calcium-bearing minerals condense with the same isotopic composition if there is minimal mass fractionation during the condensation process. The lack of calcium isotopic fractionation during condensation is demonstrated by the absence of calcium mass fractionation effects in normal Allende inclusions. The major weakness of the model, however, is that there is no explanation of how the exotic reservoir became mass fractionated. One way of making such a gas was discussed by Lee *et al.* (1980). They envisioned hot, ionized supernova ejecta in which temperatures are so high that all elements exist as ionized, monatomic species. They suggested that interaction of a magnetic field with such matter would cause isotopic mass fractionation, with the isotopic fractionation per a.m.u. being inversely proportional to atomic mass. In discussing this hypothesis as a possible model for the origin of HAL, Lee *et al.* grouped HAL with the FUN inclusions C1 and EK1-4-1 under the assumption that a single process was responsible for the mass fractionation in all three inclusions. They then rejected this hypothesis for HAL on the grounds that magnesium is more fractionated than oxygen in C1 and EK1-4-1. Aside from the fact that all three inclusions exhibit mass fractionation effects in major elements, however, there is little justification for grouping HAL with the other FUN inclusions. HAL differs markedly from them in textures and in mineralogical, chemical and isotopic composition, suggesting that they may have quite different origins. It may very well be that an inverse relationship exists in HAL between degree of fractionation and atomic mass, as oxygen is mass fractionated by 25‰ per a.m.u. and calcium by only 7.5‰ per a.m.u. Another way of producing a mass fractionated reservoir is to allow gaseous supernova ejecta to expand over a great distance. Since lighter atoms or molecules have greater velocities, the portion of the gas that expands the greatest distance will be light isotope-enriched and the portion that travels the least distance will be heavy isotope-enriched.

Both of the proposed mechanisms for mass fractionation operate on supernova ejecta. As we have seen, the only supernova ejecta having both the oxidizing conditions and near-chondritic relative chemical abundances required for formation of HAL are found in hydrogen- and helium-burning zones. During hydrogen-burning through the CNO cycle, oxygen isotopes are burned in reactions which produce ^{14}N. Because of the relatively slow rate of the reaction $^{17}O(p, \alpha)^{14}N$ (Rolfs and Rodney, 1975), the $^{17}O/^{16}O$ ratio in a hydrogen-burning zone should be much higher than the terrestrial ratio. This is inconsistent with the observed oxygen isotopic composition of HAL, which is moderately enriched in ^{16}O relative to terrestrial oxygen. Furthermore, during high-temperature helium-burning, free neutrons are released which react to produce very large $^{44}Ca/^{40}Ca$ ratios compared to the terrestrial value (Lamb *et al.*, 1977). These have not been observed in HAL either. Thus, the only type of supernova ejecta from a single shell which satisfies all of the chemical and isotopic constraints is that from a low temperature helium-burning zone. It is also possible that certain mixtures of material from different shells would have compositions compatible with both the chemical and isotopic constraints.

The non-mass dependent isotope anomalies in oxygen and calcium require condensation from a gas with a special nucleosynthetic history. It is likely that this gas was in a protostar or near a star in order for it to have been dense enough to allow condensation to occur. Magnetic field interactions or expansion of the gas away from the star could have been responsible for mass fractionating the gas prior to condensation. If the gas were not from the interior of a supernova, it is not likely to have been free of hydrogen and, consequently, condensation is not likely to have occurred under oxidizing conditions. In this case, a second gas-solid fractionation event is required, this one in an oxidizing environment. This could have been produced by volatilization of these pre-existing grains, a process which may or may not

have been responsible for the mass fractionation. There are two possibilities at this stage. In the first, volatilization was slow enough that the residual grains could equilibrate with one another chemically and isotopically prior to accretion of HAL. The europium fractionation could have been produced if grains of the REE-bearing component in rims were heated to a higher temperature than hibonite. In the second, volatilization was complete and the constituent grains of HAL condensed from the resulting gas at different temperatures.

Both proposed origins for HAL are compatible with the absence of ^{26}Al at the time of HAL's formation. ^{26}Al is not made in significant quantities during helium-burning, so a condensate from ejecta from the low temperature helium-burning zone of a supernova should not contain measurable ^{26}Al. If HAL formed by evaporation of interstellar grains, any ^{26}Al once present in those grains could have decayed long before volatilization occurred. Furthermore, any ^{26}Mg so produced would have been lost along with common magnesium during the vaporization process.

The extremely low cerium content of HAL implies that the gas with which HAL equilibrated did not mix with solar gas to any significant extent at the time of the final gas-solid fractionation event. The small amount of cerium seen in rim samples can be attributed to contamination of them by small amounts of normal solar material during alteration.

Acknowledgements—We thank J. M. Lattimer for the use of unpublished data and for performing new calculations on C1 chondritic gases, J. M. Allen for the use of unpublished electron microprobe analyses of HAL and B. Mason and H. Palme for the use of unpublished analyses of volatile elements in coarse-grained inclusions. We are grateful for valuable discussions with J. M. Allen, R. N. Clayton, I. Kawabe and G. J. MacPherson. We thank W. V. Boynton and H. Palme for their thorough reviews of this paper. This work was supported by funds from the National Aeronautics and Space Administration through grants NGR 14-001-249 (L.G.) and NGL 05-002-188 (G.J.W.), the Alfred P. Sloan Research Foundation (L.G.) and the Enrico Fermi Institute and Robert R. McCormick Trust (T.L.). Parts of this paper were written by L.G. while on leave at the Hebrew University of Jerusalem where he was supported by funds from the Lady Davis Fellowship Trust and funds from Mr. Lester M. Finkelstein.

REFERENCES

Ackermann R. J. and Chandrasekharaiah M. S. (1975) Systematic thermodynamic properties of actinide metal-oxygen systems at high temperatures. In *Thermodynamics of Nuclear Materials 1974, Vol. II*, pp. 3–26. International Atomic Energy Agency.

Ackermann R. J. and Rauh E. G. (1974) Thermodynamic properties of ZrO(g) and HfO(g); a critical examination of isomolecular oxygen-exchange reactions. *J. Chem. Phys.* **60**, 2266–2271.

Allen J. M., Grossman L., Davis A. M. and Hutcheon I. D. (1978) Mineralogy, textures and mode of formation of a hibonite-bearing Allende inclusion. In *Proc. Lunar Planet. Sci. Conf. 9th*, Houston, Vol. 1, pp. 1209–1233. Pergamon Press.

Allen J. M., Grossman L., Lee T. and Wasserburg G. J. (1980) Mineralogy and petrography of HAL, an isotopically-unusual Allende inclusion. *Geochim. Cosmochim. Acta* **44**, 685–699.

Ames L. L., Walsh P. N. and White D. (1967) Rare earths. IV. Dissociation energies of the gaseous monoxides of the rare earths. *J. Phys. Chem.* **71**, 2707–2718.

Bar-Matthews M., Hutcheon I. D., MacPherson G. J. and Grossman L. (1982) A corundum-rich inclusion in the Murchison carbonaceous chondrite. *Geochim. Cosmochim. Acta* **46**, 31–41.

Bowman W. W. and McMurdo K. W. (1974) Radioactive-decay gammas ordered by energy and nuclide. *At. Data Nucl. Data Tables* **13**, 89–292.

Boynton W. V. (1975) Fractionation in the solar nebula: condensation of yttrium and the rare earth elements. *Geochim. Cosmochim. Acta* **39**, 569–584.

Boynton W. V. (1978) Rare-earth elements as indicators of supernova condensation (abstract). In *Lunar and Planetary Science* **IX**, pp. 120–122. The Lunar and Planetary Institute.

Boynton W. V. and Cunningham C. C. (1981) Condensation of refractory lithophile trace elements in the solar nebula and in supernovae (abstract). In *Lunar and Planetary Science* **XII**, pp. 106–108. The Lunar and Planetary Institute.

Chandrasekharaiah M. S. (1967) Volatilities of refractory inorganic compounds. In *The Characterization of High-Temperature Vapors* (ed. J. L. Margrave), pp. 495–507. Wiley.

Chase M. W., Cornutt J. L., Hu A. T., Prophet H., Sylverud A. N. and Walker L. C. (1974) JANAF thermochemical tables, 1974 supplement. *J. Phys. Chem. Ref. Data* **3**, 311–480.

Chase M. W., Cornutt J. L., Prophet H., McDonald R. A. and Sylverud A. N. (1975) JANAF thermochemical tables, 1975 supplement. *J. Phys. Chem. Ref. Data* **4**, 1–175.

Chen J. H. and Tilton G. R. (1976) Isotopic lead investigations on the Allende carbonaceous chondrite. *Geochim. Cosmochim. Acta* **40**, 635–643.

Chen J. H. and Wasserburg G. J. (1981) The isotopic composition of uranium and lead in Allende inclusions and meteoritic phosphates. *Earth Planet. Sci. Lett.* **52**, 1–15.

Chou C.-L., Baedecker P. A. and Wasson J. T. (1976) Allende inclusions: volatile-element distribution and evidence for incomplete volatilization of presolar solids. *Geochim. Cosmochim. Acta* **40**, 85–94.

Conard R. (1976) A study of the chemical composition of Ca-Al-rich inclusions from the Allende meteorite. M. S. Thesis. Oregon State University.

Cosmovici C. B., D'Anna E., D'Innocenzo A., Leggieri G., Perrone A. and Dirscherl T. (1977) The reaction Yb + O_2 → YbO + O in a crossed molecular beam experiment. *Chem. Phys. Lett.* **47**, 241–244.

Davis A. M. and Grossman L. (1979) Condensation and fractionation of rare earths in the solar nebula. *Geochim. Cosmochim. Acta* **43**, 1611–1632.

Davis A. M., Grossman L. and Allen J. M. (1978) Major and trace element chemistry of separated fragments from a hibonite-bearing Allende inclusion. In *Proc. Lunar Planet. Sci. Conf. 9th*, Houston, Vol. 1, pp. 1235–1247. Pergamon Press.

Dreibus G., Spettel B. and Wänke H. (1979) Halogens in meteorites and their primordial abundances. In *Origin and Distribution of the Elements* (ed. L. H. Ahrens), pp. 33–38. Pergamon Press.

Ganapathy R., Papia G. M. and Grossman L. (1976) The abundances of zirconium and hafnium in the solar system. *Earth Planet. Sci. Lett.* **29**, 302–308.

Gast P. W., Hubbard N. J. and Wiesmann H. (1970) Chemical composition and petrogenesis of basalts from

Tranquillity Base. In *Proc. Apollo 11 Lunar Sci. Conf.*, Houston, Vol. 2, pp. 1143–1163. Pergamon Press.

Grossman L. (1973) Refractory trace elements in Ca-Al-rich inclusions in the Allende meteorite. *Geochim. Cosmochim. Acta* **37,** 1119–1140.

Grossman L. (1975) Petrography and mineral chemistry of Ca-rich inclusions in the Allende meteorite. *Geochim. Cosmochim. Acta* **39,** 433–454.

Grossman L. and Ganapathy R. (1975) Volatile elements in Allende inclusions. In *Proc. Lunar Sci. Conf. 6th*, Houston, Vol. 2, pp. 1729–1736. Pergamon Press.

Grossman L. and Ganapathy R. (1976a) Trace elements in the Allende meteorite-I. Coarse-grained, Ca-rich inclusions. *Geochim. Cosmochim. Acta* **40,** 331–344.

Grossman L. and Ganapathy R. (1976b) Trace elements in the Allende meteorite-II. Fine-grained, Ca-rich inclusions. *Geochim. Cosmochim. Acta* **40,** 967–977.

Grossman L., Ganapathy R. and Davis A. M. (1977) Trace elements in the Allende meteorite-III. Coarse-grained inclusions revisited. *Geochim. Cosmochim. Acta* **41,** 1647–1664.

Grossman L., Olsen E., Davis A. M., Tanaka T. and MacPherson G. J. (1981) The Antarctic achondrite ALHA 76005: a polymict eucrite. *Geochim. Cosmochim. Acta* **45,** 1267–1279.

Gschneidner K. A. Jr., Kippenhan N. and McMasters O. D. (1973) Thermochemistry of the rare earths. Part I. Rare earth oxides. Report IS-RIC-6. Rare-Earth Information Center, Ames, Iowa, 67 p.

Hildenbrand D. L. (1977) Dissociation energy of samarium monoxide and its relation to that of europium monoxide. *Chem. Phys. Lett.* **48,** 340–344.

Hultgren, R., Desai P. D., Hawkins D. T., Gleiser M., Kelley K. K. and Wagman D. D. (1973) *Selected Values of the Thermodynamic Properties of the Elements.* American Society for Metals, 636 p.

JANAF Thermochemical Tables (1977) Supplement No. 47. Compiled by the Thermal Research Laboratory, Dow Chemical Company, Midland, Michigan.

Jarosewich E. and Clarke R. S. Jr. (1980) The Allende meteorite reference sample. *Smithson. Contrib. Earth Sci.*, (in press).

Keays R. R., Ganapathy R., Laul J. C., Krähenbühl U. and Morgan J. W. (1974) The simultaneous determination of 20 trace elements in terrestrial, lunar and meteoritic material by radiochemical neutron activation analysis. *Anal. Chim. Acta* **72,** 1–29.

Keil K. and Fuchs L. H. (1971) Hibonite [$Ca_2(Al,Ti)_{24}O_{38}$] from the Leoville and Allende chondritic meteorites. *Earth Planet. Sci. Lett.* **12,** 184–190.

Kordis J. and Gingerich K. A. (1977) Mass spectrometric observations of some polyatomic gaseous rare earth oxides and their atomization energies. *J. Chem. Phys.* **66,** 483–491.

Kramar U. (1980) The importance of second order activation in the determination of trace elements in geological samples by instrumental neutron activation analysis. *Geochim. Cosmochim. Acta* **44,** 379–382.

Lamb S. A., Howard W. M., Truran J. W. and Iben I. Jr. (1977) Neutron-capture nucleosynthesis in the helium-burning cores of massive stars. *Astrophys. J.* **217,** 213–221.

Lattimer J. M. and Grossman L. (1978) Chemical condensation sequences in supernova ejecta. *Moon and Planets* **19,** 169–184.

Lattimer J. M., Schramm D. N. and Grossman L. (1978) Condensation in supernova ejecta and isotopic anomalies in meteorites. *Astrophys. J.* **219,** 230–249.

Lederer C. M., Hollander J. M. and Perlman I. (1967) *Table of Isotopes*, 6th edition. Wiley, 594 p.

Lee T., Mayeda T. K. and Clayton R. N. (1980) Oxygen isotopic anomalies in Allende inclusion HAL. *Geophys. Res. Lett.* **7,** 493–496.

Lee T., Russell W. A. and Wasserburg G. J. (1979) Calcium isotopic anomalies and the lack of aluminum-26 in an unusual Allende inclusion. *Astrophys. J. Lett.* **228,** L93–L98.

Martin P. M. and Mason B. (1974) Major and trace elements in the Allende meteorite. *Nature* **249,** 333–334.

Mason B. and Martin P. M. (1977) Geochemical differences among components of the Allende meteorite. *Smithson. Contrib. Earth Sci.*, No. 19, pp. 84–95.

Murad E. (1978) The dissociation energies of gaseous praseodymium- and neodymium-oxides and their structure. *Chem. Phys. Lett.* **59,** 359–361.

Murad E. and Hildenbrand D. L. (1975) Thermochemical properties of gaseous ZrO and ZrO_2. *J. Chem. Phys.* **63,** 1133–1139.

Murad E. and Hildenbrand D. L. (1976) Thermochemical properties of gaseous EuO. *J. Chem. Phys.* **65,** 3250–3256.

Nagasawa H., Blanchard D. P., Jacobs J. W., Brannon J. C., Philpotts J. A. and Onuma N. (1977) Trace element distribution in mineral separates of the Allende inclusions and their genetic implications. *Geochim. Cosmochim. Acta* **41,** 1587–1600.

Nagasawa H. and Onuma N. (1979) High temperature heating of the Allende meteorite II. Fractionation of the rare earth elements (abstract). In *Lunar and Planetary Science X*, pp. 884–886. The Lunar and Planetary Institute.

Nagasawa H., Schreiber H. D. and Morris R. V. (1980) Experimental mineral/liquid partition coefficients of the rare earth elements (REE), Sc and Sr for perovskite, spinel and melilite. *Earth Planet. Sci. Lett.* **46,** 431–437.

Nakamura N. (1974) Determination of REE, Ba, Fe, Mg, Na and K in carbonaceous and ordinary chondrites. *Geochim. Cosmochim. Acta* **38,** 757–775.

Nuclear Data Sheets (Sept. 1980 and earlier). Edited by Nuclear Data Group, Oak Ridge National Laboratory, Oak Ridge, Tennessee.

Notsu K., Onuma N. and Nishida N. (1978) High temperature heating of the Allende meteorite. *Geochim Cosmochim. Acta* **42,** 903–907.

Palme H. and Wlotzka F. (1976) A metal particle from a Ca, Al-rich inclusion from the meteorite Allende, and the condensation behavior of refractory siderophile elements. *Earth Planet. Sci. Lett.* **33,** 45–60.

Perlman I. and Asaro F. (1969) Pottery analysis by neutron activation. *Archaeometry* **11,** 21–52.

Perlman I. and Asaro F. (1971) Pottery analysis by neutron activation. In *Science and Archaeology* (ed. R. H. Brill), pp. 182–195. MIT Press.

Robie R. A., Hemingway B. S. and Fisher J. R. (1978) *Thermodynamic Properties of Minerals and Related Substances at 298.15 K and 1 Bar (10^5 Pascals) Pressure and at Higher Temperature.* U. S. Geol. Surv. Bull. 1452, U. S. Govt. Printing Office, 456 p.

Rolfs C. and Rodney W. S. (1975) Hydrogen burning of ^{17}O in the CNO cycle. *Nuclear Physics* **A250,** 295–308.

Shannon R. D. (1976) Revised effective ionic radii and systematic studies of interatomic distances in halides and chalcogenides. *Acta Cryst.* **A32,** 751–767.

Shima M. (1979) The abundances of titanium, zirconium and hafnium in stony meteorites. *Geochim. Cosmochim. Acta* **43,** 353–362.

Stull D. R. and Prophet H. (1971) *JANAF Thermochemical Tables.* Natl. Standard Ref. Data Ser., U. S. Natl. Bur. Standards, Vol. 37, U. S. Govt. Printing Office, 1141 p.

Tanaka T., Davis A. M., Grossman L., Lattimer J. M., Allen J. M., Lee T. and Wasserburg G. J. (1979) Chemical study of an isotopically-unusual Allende inclusion (abstract). In *Lunar and Planetary Science* **X,** pp. 1203–1205. The Lunar and Planetary Institute.

Tatsumoto M., Unruh D. M. and Desborough G. A. (1976)

U-Th-Pb and Rb-Sr systematics of Allende and U-Th-Pb systematics of Orgueil. *Geochim. Cosmochim. Acta* **40,** 617–634.

Walker F. W., Kirouac G. J. and Rourke F. M. (1977) *Chart of the Nuclides*, 12th edition. General Electric Company.

Wänke H., Baddenhausen H., Palme H. and Spettel B. (1974) On the chemistry of the Allende inclusions and their origin as high temperature condensates. *Earth Planet. Sci. Lett.* **23,** 1–7.

Wark D. A. and Lovering J. F. (1976) Refractory/platinum metal grains in Allende calcium-aluminium-rich clasts (CARC's): possible exotic presolar material? (abstract). In *Lunar Science* **VII,** 976–978. The Lunar Science Institute.

Wark D. A. and Wasserburg G. J. (1980) Anomalous mineral chemistry of Allende FUN inclusions C1, EK-141 and EGG 3 (abstract). In *Lunar and Planetary Science* **XI,** pp. 1214–1216. The Lunar and Planetary Institute.

Wasserburg G. J., Lee T. and Papanastassiou D. A. (1977) Correlated O and Mg isotopic anomalies in Allende inclusions: II. Magnesium. *Geophys. Res. Lett.* **4,** 299–302.

APPENDIX

Short INAA irradiation

Using the instrumental neutron activation analysis (INAA) procedure of Davis *et al.* (1978) for major element analysis of submilligram samples, the fragments of HAL were sealed into tiny polyethylene pouches. The samples described in the Experimental section, some other Allende samples, three empty pouches, Standard Pottery SP (Perlman and Asaro, 1969), USGS standard rock BCR-1 and Johnson-Matthey Specpure MgO, Al_2O_3, SiO_2, $CaCO_3$ and TiO_2 were individually irradiated in the first row of the graphite reflector of the University of Missouri Research Reactor (MURR) for 5 min at a flux of 1.0×10^{14} neutrons cm^{-2} sec^{-1} using the pneumatic transfer system. After each irradiation, the pouch was removed from the rabbit and taped to an aluminum counting card, so that all samples and standards could be counted in exactly the same geometry. After a decay period of 10 min, each sample was counted for 500 sec for ^{27}Mg, ^{28}Al, ^{49}Ca, ^{51}Ti and ^{52}V using a Ge-Li detector. After decay times of 1.5 to 3.5 hr, the samples were counted for 1000 sec each for ^{24}Na, ^{56}Mn and ^{165}Dy. Variations in neutron flux throughout the run were monitored by periodically irradiating gold-doped aluminum wires and counting ^{198}Au several days later. Since the specific activity of ^{198}Au varied by less than 2% throughout the run, no flux corrections were necessary. The Specpure MgO, Al_2O_3 and SiO_2 were used to correct for the following fast neutron reactions: $^{24}Mg(n,p)^{24}Na$; $^{27}Al(n,\alpha)^{24}Na$; $^{27}Al(n,p)^{27}Mg$ and $^{28}Si(n,p)^{28}Al$.

Long INAA irradiation

The samples were transferred from the polyethylene pouches to Suprasil quartz vials and the vials were sealed with a gas-oxygen torch. The vials containing the samples, SP, BCR-1 and four group chemical standards, Os-Ru, Au-Ir-Re, Ag-Ni-Pd-Pt-Se-Zn and REE, were individually wrapped in household aluminum foil. The chemical standards other than REE were prepared essentially as described by Keays *et al.* (1974). Stock solutions from which the REE standard was prepared were made with great caution, because lanthanide oxides are subject to absorption and adsorption of atmospheric water and carbon dioxide (Gast *et al.*, 1970). A solution of each lanthanide was prepared by dissolving its Johnson-Matthey Specpure oxide in nitric acid. The concentrations of these solutions were checked by EDTA back titrations using a zinc standard solution. The REE standard was prepared by combining, diluting and evaporating stock solutions such that it had approximately chondritic relative proportions of all REE.

The samples and standards were irradiated in the flux trap of the MURR for 105.7 hr at a flux of 5.6×10^{14} neutrons cm^{-2} sec^{-1}. Variations in neutron flux were monitored by counting ^{59}Fe, produced from ^{58}Fe by thermal neutron capture, and ^{54}Mn, produced by the fast neutron reaction $^{54}Fe(n,p)^{54}Mn$, in the aluminum foil surrounding each vial. The maximum deviation from the average neutron flux was 7%. This flux correction method was described in detail by Grossman *et al.* (1981). After three days, the quartz vials were washed in hot nitric acid and aqua regia and the samples were transferred from them into new quartz vials and counted on high resolution Ge-Li detectors. Each sample was counted 5 times: (1) for 2.5 to 15 hr each; (2) until the highest peak reached 10^6 counts; (3) until the highest part of the background reached 5×10^5 counts, 1.5 to 7 days each; (4) and (5) 2 to 7 days each, 6 and 10 months, respectively, after the irradiation. We found that all REE in SP were depleted by nearly the same amount, 16.7%, compared to the results of Perlman and Asaro (1971) and that all REE in BCR-1 were depleted by 29.0% relative to the data of Nakamura (1974). Therefore, we used these average REE depletions to correct all other elements in these standards for transport loss. Due to insufficient cooling during the irradiation, the Ag-Ni-Pd-Pt-Se-Zn standard was destroyed. No contamination by the elements in this standard was noted in either the samples or in the aluminum foils surrounding their vials.

Calcium was the only element determined in both short and long INAA irradiations. Sample 1, a single piece of hibonite prior to the long irradiation, was found to contain substantially less calcium after the long irradiation than after the short. Comparison of the hibonite chip counted after the long irradiation with photographs of the sample taken prior to the short irradiation revealed that the sample had split and a large portion was lost during transfer following the long irradiation. The sample was reweighed, bringing the two calcium determinations into agreement with one another. The portion of sample 1 retained after the long irradiation contained both clear and frosty hibonite, as did the original sample. Occasionally, small amounts of water were found in sealed quartz vials, presumably from the torch used to seal them. Samples 5 and 6 contained a yellow liquid after the long irradiation. These samples were rinsed with distilled water and transferred to clean vials, but we fear that some leaching has taken place. These samples could not be reweighed, because they were broken into several small fragments during the long irradiation. Comparison of calcium contents determined in both INAA irradiations confirmed that substantial portions of samples 5 and 6 had been lost: 53 and 38%, respectively. This difference was used to correct for transport loss. No loss of the remaining samples was indicated from their calcium contents determined in the two INAA irradiations.

Zinc was determined from the 1115.5 keV line of ^{65}Zn. Since this small peak lay directly below a very large peak at 1120.5 keV from ^{46}Sc, uncertainty in the degree of curvature of the background led to a larger uncertainty in the area of the ^{65}Zn peak than was indicated by counting statistics alone. Multichannel analyzer data for the ^{65}Zn peak were plotted and the shape of the background was drawn to be similar to that of sample 1, which had no discernible ^{65}Zn peak. We have arbitrarily assigned an uncertainty of 20% to the zinc data.

Zirconium was determined using the 756.7 keV line of ^{95}Zr. An important interference came from the 756.8 keV line of ^{154}Eu. The ratio of the specific activity of the 756.8 keV line of ^{154}Eu to that of the 1408.0 keV line of ^{152}Eu was determined in the REE standard and used to correct for ^{154}Eu contributions to the 756.7 keV peaks of samples. Since most of the samples have high zirconium/europium

ratios, the corrections ranged from 6 to 9% of the total peak area.

The sum of silica, phosphorus pentoxide and sulfur was determined by subtracting from 100% the sum of elemental ruthenium, osmium, iridium and gold and the oxides of all other measured elements. Iron and vanadium were assumed to be present as FeO and V_2O_5, respectively.

RNAA irradiation

Although up to 10 REE can be determined by INAA when levels are sufficiently high, REE were determined by radiochemical neutron activation analysis (RNAA) to reduce the Compton background and other interference effects of non-REE radionuclides. The radiochemical separation scheme used was that of Conard (1976) for REE, barium and strontium. After completion of counting following the long INAA irradiation, samples 1, 2, 3, 4 and 7 and standards SP, BCR-1 and REE were irradiated in the flux trap of the MURR for 143.6 hr at a flux of 6.02×10^{14} neutrons Cm^{-2} sec^{-1}. The standards used were from the INAA irradiation, so that samples and standards had the same neutron irradiation history. For this irradiation, the rabbit was a solid aluminum block with several cylindrical holes slightly larger in diameter than the quartz vials. Two vials were placed in each hole. Neutron flux variations were monitored by counting ^{60}Co from cobalt-doped aluminum wires that were inserted into four holes parallel to those containing the sample vials. The maximum deviation from the average neutron flux was 6%.

REE carriers were prepared from their isotopically normal Johnson-Matthey Specpure oxides and from isotopically enriched oxides from Oak Ridge National Laboratory, following the procedure of Conard (1976). Relative amounts of REE in the carrier were chosen to provide equal count rates for most REE when chemical yields are determined by reactivation. To enhance the counting statistics for ^{149}Nd and ^{177}Yb, neodymium oxide enriched in ^{148}Nd and ytterbium oxide enriched in ^{176}Yb were added to the carrier solution. Also, to reduce the interference of the 104.3 keV line of ^{155}Sm ($T_{1/2}$ = 22.1 min) on the 103.2 keV line of ^{153}Sm, samarium enriched in ^{152}Sm was used instead of isotopically normal samarium. Carriers for barium and strontium were prepared from their Johnson-Matthey Specpure carbonates.

After two days of decay, the quartz irradiation vials were washed in aqua regia and opened and the samples were transferred to nickel crucibles to which carriers had previously been added. Sample loss during the transfer was monitored by counting ^{46}Sc in each vial before and after removal of the sample or standard. The only significant losses were for SP and BCR-1, which lost 17.6 and 8.2% of their masses, respectively. In order to ensure recovery of any REE that may have been implanted into the quartz vial during the irradiations, the REE standard was fused in its quartz vial. An irradiated empty vial was fused to determine blank corrections for the REE standards. These corrections were negligible.

The samples and standards were fused with 4 g of sodium peroxide and 4 sodium hydroxide pellets. Using a terrestrial hibonite chip, we determined that a 40 min fusion was sufficient for complete dissolution of hibonite. The chemical procedure for separation of barium, strontium and REE was that of Conard (1976) and is only summarized here. The fusion cakes were dissolved in water, acidified with hydrochloric acid and barium and strontium were precipitated as sulfates with sulfuric acid. The REE were precipitated as hydroxides with ammonium hydroxide and then purified by alternately precipitating as fluorides and hydroxides. This cycle was repeated at least six times for each sample and, prior to mounting the REE separate, ^{46}Sc activity was measured to test the efficiency of removal of scandium. ^{46}Sc is the most important unwanted radionuclide in REE separates from Allende inclusions. Further purification of barium and strontium followed the procedures of Conard (1976) and Grossman *et al.* (1977).

In order to obtain a favorable counting geometry, the final REE hydroxide precipitate was dissolved in a minimum amount of nitric acid and the resulting solution evaporated onto a glass fiber filter disk under a heat lamp. The samples were then counted using high resolution Ge-Li detectors. The samples were counted 4 times: (1) for 3 to 6 hr each, starting 4 days after the end of the irradiation; (2) until the highest peak reached 10^6 counts, 0.5 to 2 days each; (3) 4 to 7 days each; and (4) 6 to 7 days each, 2 to 3 months later. ^{85}Sr activities in the final $SrCO_3$ precipitates were measured on a 2×2 inch NaI detector. The final $BaCrO_4$ precipitates were counted on high resolution Ge-Li detectors to allow determination of barium, using ^{140}Ba, and uranium, using the daughter product of ^{140}Ba, ^{140}La. ^{140}Ba is produced in the reactor by $^{238}U(n,f)^{140}Ba$.

There are a number of unusual interferences caused by the anomalous REE patterns in our samples and by the extremely high neutron fluence used (5.24×10^{20} neutrons cm^{-2}). These interferences are dealt with below.

Cerium was determined *via* the 145.4 keV line of ^{141}Ce. Because HAL has extremely low cerium concentrations, the 144.9 keV line of ^{175}Yb interfered in early counts. The 144.9/396.3 keV peak area ratio of ^{175}Yb was determined from a cerium-free ytterbium standard included in a later irradiation and was used to correct the total 145.4 keV peak area for the ^{175}Yb contribution in all samples and standards. The HAL samples had very high lanthanum/cerium ratios, so that a normally insignificant lanthanum interference on cerium determinations became important in the HAL samples. Under conditions of high neutron fluence, some ^{141}Ce was produced from ^{139}La *via* the following reaction chains: (1) $^{139}La(n,\gamma)^{140}La(n,\gamma)^{141}La(\beta^-)^{141}Ce$ and (2) $^{139}La(n,\gamma)^{140}La(\beta^-)^{140}Ce(n,\gamma)^{141}Ce$. In addition, ^{140}Ce was produced from decay of ^{140}La following the long INAA irradiation. This ^{140}Ce, along with ^{140}Ce produced from ^{139}La *via* chain (2) in the long INAA irradiation, was then activated in the RNAA irradiation. Using half-lives and neutron capture cross-sections of Walker *et al.* (1977) with the cadmium ratio of 14 for our irradiation position in the MURR, we calculated that after the long INAA irradiation, 1 μg lanthanum ≡ 0.0087 μg cerium and after the RNAA irradiation, 1 μg lanthanum ≡ 0.0138 μg cerium. These corrections were applied to all samples and standards. The lanthanum and ytterbium corrections accounted for all of the 145.4 keV γ-ray counts in samples 1 and 2 and for 64, 90 and 15% of the 145.4 keV γ-ray counts in samples 3, 4 and 7, respectively.

Samarium was determined *via* the 103.2 keV line of ^{153}Sm. Under conditions of high neutron fluence, ^{153}Sm was also produced from ^{151}Eu by the following reaction: $^{151}Eu(n,\gamma)^{152m1}Eu(EC)^{152}Sm(n,\gamma)^{153}Sm$. In addition, some ^{152}Sm was produced by decay of $^{152m1}Eu$ after the long INAA irradiation. This ^{152}Sm, along with ^{152}Sm produced from ^{151}Eu by the above reaction chain, was then activated in the RNAA irradiation. Using half-lives and neutron capture cross-sections of Walker *et al.* (1977) and the $^{152m1}Eu$ branching ratio of Lederer *et al.* (1967), we calculated that after the long INAA irradiation, 1 μg europium ≡ 0.081 μg samarium and after the RNAA irradiation, 1 μg europium ≡ 0.162 μg samarium. Corrections for this effect were applied to all samples and standards. For a sample with a chondritic europium/samarium ratio, the correction was 6% for the RNAA irradiation. Another minor correction was necessary for the samarium data. A small contribution (~1%) to the total 103.2 keV peak area came from the 103.2 keV line of ^{153}Gd ($T_{1/2}$ = 242 days). The ^{153}Gd count rate for this peak was measured after complete decay of ^{153}Sm. The decay-corrected ^{153}Gd contribution was then subtracted from the total 103.2 keV peak area in early counts.

Europium was determined *via* the 1408.0 keV line of ^{152}Eu. This isotope has a very high neutron capture cross-section, 13000 barns, so that a significant fraction of the total ^{152}Eu produced in the reactor undergoes neutron capture to form stable ^{153}Eu. ^{151}Eu also has a large neutron capture cross-section, 9000 barns, so that only 13.4% of the ^{151}Eu remained after the long INAA irradiation and 0.71% remained after the subsequent RNAA irradiation. These high cross-sections led to the effect that the specific activity of ^{152}Eu was higher by a factor of 12 after the long INAA irradiation than after the RNAA irradiation. The high cross-sections and large neutron fluences also led to the unusual effect that, for a given irradiation time, increased flux produced decreased ^{152}Eu specific activity. Thus, for europium, the correction for flux differences between samples and standards had to be calculated in a different way from that described above for other elements. For each sample, the flux correction was applied to the neutron flux in each irradiation and the amount of ^{152}Eu produced per μg of europium was calculated using half-lives and cross-sections from Walker *et al.* (1977). The flux corrections so calculated for the INAA irradiation were small since all samples and the REE standard were irradiated on the same layer and received nearly the same flux.

Gadolinium is frequently determined *via* long-lived ^{153}Gd in both INAA and RNAA. Kramar (1980) cautioned against using this isotope for gadolinium determination when high neutron fluences are used because ^{153}Gd can also be made from europium by the following reaction chain: ^{151}Eu(n,γ)^{152m1}Eu(β^-)^{152}Gd(n,γ)^{153}Gd. Because ^{151}Eu is an abundant isotope of europium, ^{152}Gd is a rare isotope of gadolinium and the neutron capture cross-section of ^{151}Eu is extremely high, considerably more ^{153}Gd was produced from europium than from gadolinium during the long INAA irradiation. ^{152}Gd was also produced from the decay of ^{152m1}Eu during and after the long INAA irradiation. This ^{152}Gd was then activated in the RNAA irradiation. Using half-lives and cross-sections from Walker *et al.* (1977) and the ^{152m1}Eu branching ratio of Lederer *et al.* (1967), we calculated that after the INAA irradiation, 1 μg europium $\equiv$ 34.0 μg gadolinium and after the RNAA irradiation, 1 μg europium = 63.6 μg gadolinium. Despite the fact that gadolinium is naturally more abundant than europium, only 5% of the ^{153}Gd counts in our samples were due to gadolinium and 95% were due to europium after the RNAA irradiation. The magnitudes of the corrections for this effect, coupled with uncertainties in neutron capture cross-sections, preclude determination of gadolinium *via* ^{153}Gd. The negative gadolinium anomalies mentioned in our preliminary report (Tanaka *et al.*, 1979) were artifacts due to our failure to correct for this effect. Although gadolinium was determined in some samples using ^{159}Gd, counting statistics for this isotope are poor even for REE-rich samples.

^{166}Ho ($T_{1/2}$ = 26.8 hr) is normally used to determine holmium; however, this isotope is also produced from dysprosium *via* the following reaction chains: (1) ^{164}Dy(n,γ)^{165}Dy(n,γ)^{166}Dy(β^-)^{166}Ho; (2) ^{164}Dy(n,γ)-^{165m}Dy(IT)^{165}Dy(n,γ)^{166}Dy(β^-)^{166}Ho; (3) ^{164}Dy(n,γ)-^{165}Dy(β^-)^{165}Ho(n,γ)^{166}Ho; and (4) ^{164}Dy(n,γ)^{165m}Dy(IT)-^{165}Dy(β^-)^{165}Ho(n,γ)^{166}Ho. In both irradiations, dysprosium produced considerably more ^{166}Ho than did holmium, so that holmium could not be determined. Production of significant amounts of ^{166}Dy allowed determination of dysprosium with much better accuracy than was possible using ^{165}Dy from the short irradiation. Using half-lives and neutron capture cross-sections from Walker *et al.* (1977), neutron flux corrections to the ^{166}Dy specific activity were calculated in a similar way to those to the ^{152}Eu activity.

Thulium was determined *via* the 84.3 keV line of ^{170}Tm. In INAA, this line suffered from interference from the 84.7 keV line of ^{182}Ta. As the more intense lines of ^{182}Ta at 100.1 and 1221.4 keV were not detected after the radiochemical separation, no correction was necessary.

Lutetium was determined *via* the 208.4 keV line of ^{177}Lu. Lutetium determination by this isotope is known to suffer from interference from ^{177}Lu produced by the decay of ytterbium-produced ^{177}Yb. Corrections for this interference were applied in the way discussed in Grossman *et al.* (1977). The extremely high scandium content of the HAL samples led to another important interference that was significant for samples low in lutetium even when the bulk of the scandium was removed by radiochemical separation. Compton backscattered γ-rays from interaction of 889.3 keV ^{46}Sc γ-rays with the lead shield surrounding the Ge-Li detector produced a broad bump in the background. The energy of the backscattered γ-rays was dependent on the geometry of the shield and, for the shields surrounding our detectors, the bump reached a maximum at about 210 keV. As a result, integration of the 208.4 keV region for determination of lutetium gave a significant number of counts even in the absence of any real ^{177}Lu peak. By examining counts made long after the decay of ^{177}Lu, it was determined that the apparent peak area produced by Compton backscatter is proportional to the area of the 889.3 keV peak of ^{46}Sc. The ratio of areas of these two peaks was determined for each detector by counting a ^{46}Sc source in the geometry used for the lutetium counts. This ratio was used to correct the earlier counts for the contribution of backscattered ^{46}Sc γ-rays. Uncertainties due to counting statistics as well as those due to variation of the backscatter/889.3 keV peak area ratio among the several measurements made were carried through the calculation of final lutetium concentrations. The corrections ranged from 0.4 to 20.1% of the total 208.4 keV peak area ratio.

Chemical yields

The chemical yields of barium and strontium were determined by gravimetry and had ranges of 52 to 82% and 0.5 to 14.2%, respectively.

The chemical yields for REE were determined by INAA. The glass fiber filter disks upon which the nitric acid solutions of REE had been evaporated contained substantial amounts of sodium, so it was necessary to remove the REE from the disks. This was done by repeated leaching of the disks with 6N nitric acid. The resulting solutions were diluted to exactly 25 ml with 6N nitric acid. One ml aliquots of each solution were evaporated to dryness with a heat lamp in high-density polyethylene vials. Standards were prepared in a similar manner from the REE carrier solution. The vials were heat-sealed shut and placed in irradiation rabbits, three vials per layer and three layers per rabbit. Standards were placed in the bottom and top layers of each rabbit, so that flux variations in the vertical direction could be monitored. Flux variation in the horizontal direction was not measured. Each rabbit was irradiated for 20 sec at a flux of 1.0×10^{14} neutrons cm^{-2} sec^{-1} in the graphite reflector, first row, of the MURR *via* the pneumatic transfer system. Beginning 30 min after each irradiation, each vial was counted for 1000 sec live time using a Ge-Li detector. After one day, each vial was counted closer to the detector for 1200 sec live time. Since radiochemical separation of REE is expected to produce chemical yields that vary smoothly with ionic radius, a cubic fit of chemical yield *vs.* ionic radius for these elements was made and the final chemical yields for all REE were calculated from ionic radii and regression coefficients. Chemical yields were lower for light REE than for heavy REE and ranged from 33 to 74% for lanthanum and from 43 to 98% for lutetium.